Grid diagrams and Manolescu's unoriented skein exact triangle for knot Floer homology

C-M MICHAEL WONG

We rederive Manolescu's unoriented skein exact triangle for knot Floer homology over $\mathbb{F}_2$ combinatorially using grid diagrams, and extend it to the case with $\mathbb{Z}$ coefficients by sign refinements. Iteration of the triangle gives a cube of resolutions that converges to the knot Floer homology of an oriented link. Finally, we reestablish the homological σ–thinness of quasialternating links.

1 Introduction

Heegaard Floer homology was first introduced by Ozsváth and Szabó [16] as an invariant for 3–manifolds, defined using holomorphic disks and Heegaard diagrams. It was extended by Ozsváth and Szabó [15], and independently by Rasmussen [19], to give an invariant, *knot Floer homology*, for nullhomologous knots in a closed, oriented 3–manifold, which was further generalized by Ozsváth and Szabó [18] to the case of oriented links. Knot Floer homology comes in several flavors; its most usual form, $\widehat{\mathrm{HFK}}(L)$ for an oriented link L, is a bigraded module over $\mathbb{F}_2 = \mathbb{Z}/2\mathbb{Z}$ or $\mathbb{Z}$, whose Euler characteristic is the Alexander polynomial. For the purposes of this paper, we shall only consider links in S^3.

A combinatorial description of knot Floer homology over $\mathbb{F}_2$ was given by Manolescu, Ozsváth and Sarkar [11], and Manolescu, Ozsváth, Szabó and Thurston [12], using *grid diagrams*, which are certain multipointed Heegaard diagrams on the torus. In this approach, one can associate a chain complex $\widetilde{\mathrm{GC}}(\mathbb{G})$ to a grid diagram $\mathbb{G}$, and calculate its homology $\widetilde{\mathrm{GH}}(\mathbb{G})$. Sign refinements for the boundary map ∂ are also given in [12] in a well-defined manner, allowing the chain complex to be defined over $\mathbb{Z}$. If $\mathbb{G}$ is a grid diagram for a link L of ℓ components, with *grid number* n, then

$$\widetilde{\mathrm{GH}}(\mathbb{G}) \cong \widehat{\mathrm{GH}}(L) \otimes V^{n-l},$$

where V is a free module of rank 2 over the base ring $R = \mathbb{F}_2$ or $\mathbb{Z}$, and $\widehat{\mathrm{GH}}(L)$ is a link invariant, called the *combinatorial knot Floer homology* or the *grid homology*

of L. Over $\mathbb{F}_2$, $\widehat{\mathrm{GH}}(L)$ is isomorphic to $\widehat{\mathrm{HFK}}(L)$; over $\mathbb{Z}$, it has been shown by Sarkar [21] that $\widehat{\mathrm{GH}}(L)$ is isomorphic to $\widehat{\mathrm{HFK}}(L, \mathfrak{o})$ for some orientation system $\mathfrak{o}$.

Ozsváth and Szabó [17] observed that Heegaard Floer homology of the branched double cover $\widehat{\mathrm{HF}}(-\Sigma(L))$, like Khovanov homology $\widetilde{\mathrm{Kh}}(L)$ (see Khovanov [6; 7] or Bar-Natan [3]), satisfies an unoriented skein exact triangle. Manolescu [9] then showed that over $\mathbb{F}_2$, knot Floer homology also satisfies an unoriented skein exact triangle. More precisely, let L_∞ be a link in S^3. Given a planar diagram of L_∞, let L_0 and L_1 be the two resolutions of L_∞ at a crossing in that diagram, as in Figure 1. Denote by ℓ_∞, ℓ_0 and ℓ_1 the number of components of the links L_∞, L_0 and L_1 respectively, and set $m = \max\{\ell_\infty, \ell_0, \ell_1\}$.
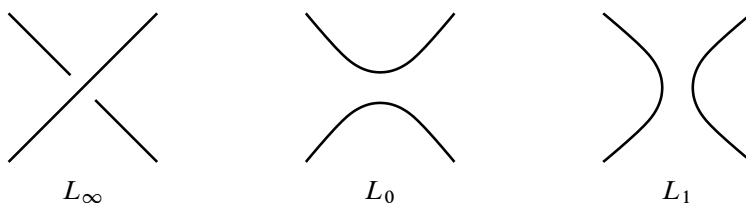

Figure 1: L_∞, L_0 and L_1 near a point

Theorem 1.1 (Manolescu) *There exists an exact triangle*

$$\cdots \to \widehat{\mathrm{HFK}}(L_\infty; \mathbb{F}_2) \otimes V^{m-\ell_\infty} \to \widehat{\mathrm{HFK}}(L_0; \mathbb{F}_2) \otimes V^{m-\ell_0}$$
$$\to \widehat{\mathrm{HFK}}(L_1; \mathbb{F}_2) \otimes V^{m-\ell_1} \to \cdots,$$

where V is a vector space of dimension 2 over $\mathbb{F}_2$.

Remark 1.2 The arrows in the exact triangle point in the reverse direction from those in [9]; this is caused by a difference in the orientation convention. We follow the convention in [15] and [11; 12], where the Heegaard surface is the oriented boundary of the handlebody in which the α curves bound discs.

Manolescu observed that the exact triangle above is different from that of $\widetilde{\mathrm{Kh}}(L)$ and $\widehat{\mathrm{HF}}(-\Sigma(L))$ in that it does not even respect the homological grading modulo 2, and that it is unclear whether an analogous triangle holds for other versions of knot Floer homology. He also used the exact triangle to show that rk $\widehat{\mathrm{HFK}}(L; \mathbb{F}_2) = 2^{\ell-1} \det(L)$ for quasialternating links, which explains the fact that $\widetilde{\mathrm{Kh}}$ and $\widehat{\mathrm{HFK}}$ have equal ranks for many classes of knots.

The goal of the present paper is to reprove Manolescu's theorem in elementary terms using grid diagrams, without appealing to the topological theory. The advantages of this approach are threefold.

First, Manolescu's skein exact triangle was proven in [9] to exist over $\mathbb{F}_2$. By assigning signs to the maps between chain complexes, we can obtain an analogous exact triangle in combinatorial knot Floer homology with $\mathbb{Z}$ coefficients, which was not known to exist before. In other words, we obtain the following statement.

Theorem 1.3 *For sufficiently large n, there exists an exact triangle*

$$\cdots \to \widehat{\mathrm{GH}}(L_\infty; R) \otimes V^{n-\ell_\infty} \to \widehat{\mathrm{GH}}(L_0; R) \otimes V^{n-\ell_0} \to \widehat{\mathrm{GH}}(L_1; R) \otimes V^{n-\ell_1} \to \cdots,$$

where $R = \mathbb{F}_2$ or $\mathbb{Z}$, and V is a free module of rank 2 over R.

Second, the exact triangle was iterated by Baldwin and Levine [2] to obtain a cube of resolutions; when using twisted coefficients, this gives a combinatorial description of knot Floer homology, distinct from that provided by grid diagrams. In the present context, knowing explicitly the maps between the chain complexes associated to the grid diagrams, we can likewise iterate the exact triangle to get a cube of resolutions complex $\mathrm{CR}(\mathbb{G})$ over $\mathbb{F}_2$, with untwisted coefficients. The higher terms in the resulting spectral sequence are combinatorially computable.

Corollary 1.4 *The cube of resolutions $\mathrm{CR}(\mathbb{G}; \mathbb{F}_2)$, which has no diagonal maps, gives rise to a spectral sequence that converges to $\widehat{\mathrm{GH}}(L; \mathbb{F}_2) \otimes V^{m-\ell}$.*

Note that the spectral sequence is presumably not a knot invariant; see [2, Remark 7.7].

The technique of spectral sequences was first used by Ozsváth and Szabó in [17], where a spectral sequence from $\widetilde{\mathrm{Kh}}(L)$ to $\widehat{\mathrm{HF}}(-\Sigma(L))$ was shown to exist. More recently, Lipshitz, Ozsváth and Thurston [8] have found a way to compute the higher terms in this spectral sequence using bordered Floer homology. Inspired by this work, Baldwin [1] has found another method of computing these higher terms.

Third, there exists a δ–*grading* on $\widehat{\mathrm{HFK}}$, and Manolescu and Ozsváth [10] investigated the δ–grading changes in the skein exact triangle [10, Proposition 3.9]. This result allowed them to apply the skein exact triangle to *quasialternating links*, to show that such links are *Floer homologically σ–thin* over $\mathbb{F}_2$. The δ–gradings can also be determined in the combinatorial picture; doing so, we prove a generalization of the statement of Floer homological σ–thinness to $\mathbb{Z}$.

Theorem 1.5 *Suppose that $\det(L_0), \det(L_1) > 0$ and $\det(L_\infty) = \det(L_0) + \det(L_1)$. Then with respect to the δ–grading, the exact sequence in Theorem 1.3 can be written as*

$$\cdots \to \widehat{\mathrm{GH}}_{*-\frac{1}{2}\sigma(L_1)}(L_1; R) \otimes V^{n-\ell_1} \to \widehat{\mathrm{GH}}_{*-\frac{1}{2}\sigma(L_\infty)}(L_\infty; R) \otimes V^{n-\ell_\infty}$$

$$\to \widehat{\mathrm{GH}}_{*-\frac{1}{2}\sigma(L_0)}(L_0; R) \otimes V^{n-\ell_0} \to \widehat{\mathrm{GH}}_{*-\frac{1}{2}\sigma(L_1)+1}(L_1; R) \otimes V^{n-\ell_1} \to \cdots,$$

where $R = \mathbb{F}_2$ or $\mathbb{Z}$, and V is a free module of rank 2 over R with grading zero.

Theorem 1.6 *Quasialternating links are Floer homologically σ–thin over $\mathbb{Z}$.*

This paper is organized as follows. We review the definition of knot Floer homology in terms of grid diagrams in Section 2, and reprove the skein exact triangle in Section 3. In these two sections, we will work only over $\mathbb{F}_2$. Sign refinements are then given in Section 4 to establish the analogous result over $\mathbb{Z}$. Next, we discuss how the exact triangle can be iterated to obtain a cube of resolutions over $\mathbb{F}_2$ in Section 5. Finally, we establish the homological σ–thinness of quasialternating links over $\mathbb{F}_2$ and $\mathbb{Z}$ in Section 6.

2 Grid diagrams

We review the combinatorial description of knot Floer homology in terms of grid diagrams. In this and the next section, we will work only over $\mathbb{F}_2 = \mathbb{Z}/2\mathbb{Z}$.

A *planar grid diagram* $\widetilde{\mathbb{G}}$ with *grid number n* is a square grid in $\mathbb{R}^2$ with $n \times n$ cells, together with a collection of Os and Xs, such that

- each row contains exactly one O and exactly one X;
- each column contains exactly one O and exactly one X; and
- each cell is either empty, contains one O, or contains one X.

Given a planar grid diagram $\widetilde{\mathbb{G}}$, we can place it in a standard position on $\mathbb{R}^2$ as follows. We place the bottom left corner at the origin, and require that each cell be a square of edge length one. We can then construct an oriented, planar link projection by drawing horizontal segments from the Os to the Xs in each row, and vertical segments from the Xs to the Os in each column. At every intersection point, we let the horizontal segment be the underpass and the vertical one the overpass. This gives a planar projection of an oriented link L onto $\mathbb{R}^2$; we say that $\widetilde{\mathbb{G}}$ is a *planar grid presentation* of L.

We transfer our grid diagram to the torus $\mathbb{T}$, by gluing the topmost segment to the bottommost one, and gluing the leftmost segment to the rightmost one. Then the horizontal and vertical arcs become horizontal and vertical circles. The torus inherits

its orientation from the plane. The resulting diagram $\mathbb{G}$ is a *toroidal grid diagram*, or simply a *grid diagram*. $\mathbb{G}$ is then a *grid presentation* of L; we also say that $\mathbb{G}$ is a grid diagram for L.

Given a toroidal grid diagram $\mathbb{G}$, we associate to it a chain complex $(\widetilde{GC}(\mathbb{G}), \partial)$ as follows. The set of generators of $\widetilde{GC}(\mathbb{G})$, denoted $S(\mathbb{G})$, consists of one-to-one correspondences between the horizontal circles and vertical circles. Equivalently, we can regard the generators as n–tuples of intersection points between the horizontal and vertical circles, such that no intersection point appears on more than one horizontal or vertical circle.

We now define the differential map $\partial\colon \widetilde{GC}(\mathbb{G}) \to \widetilde{GC}(\mathbb{G})$. Given $x, y \in S(\mathbb{G})$, let $\mathrm{Rect}(x, y)$ denote the space of embedded rectangles with the following properties. First of all, $\mathrm{Rect}(x, y)$ is empty unless x, y coincide at exactly $n - 2$ points. An element r of $\mathrm{Rect}(x, y)$ is an embedded disk in $\mathbb{T}$, whose boundary consists of four arcs, each contained in horizontal or vertical circles; under the orientation induced on the boundary of r, the horizontal arcs are oriented from a point in x to a point in y. The space of empty rectangles $r \in \mathrm{Rect}(x, y)$ with $x \cap \mathrm{Int}(r) = \varnothing$ is denoted $\mathrm{Rect}^{\circ}(x, y)$.

More generally, a *path* from x to y is a 1–cycle γ on $\mathbb{T}$ such that the boundary of the intersection of γ with the union of the horizontal curves is $y - x$, and a *domain p* from x to y is a two-chain in $\mathbb{T}$ whose boundary ∂p is a path from x to y; the set of domains from x to y is denoted $\pi(x, y)$.

Given $x \in S(\mathbb{G})$, we define

$$\partial(x) = \sum_{y \in S(\mathbb{G})} \sum_{\substack{r \in \mathrm{Rect}^{\circ}(x,y) \\ \mathrm{Int}(r) \text{ contains no } O\text{s or } X\text{s}}} y \in \widetilde{GC}(\mathbb{G}).$$

It is not too difficult to see that indeed $\partial \circ \partial = 0$, and so ∂ is a differential: we have

$$\partial \circ \partial(x) = \sum_{y \in S(\mathbb{G})} \sum_{p \in \pi(x,z)} N(p) \cdot z,$$

where $N(p)$ is the number of ways of decomposing p as a composite of two empty rectangles $p = r_1 * r_2$ with $r_1 \in \mathrm{Rect}^{\circ}(x, y)$ and $r_2 \in \mathrm{Rect}^{\circ}(y, z)$. Let $p = r_1 * r_2$; then r_1 and r_2 either are disjoint, have overlapping interiors or share a corner. If r_1 and r_2 are disjoint or have overlapping interiors, then $p = r_2 * r_1$; if they share a corner, then there exists a unique alternate decomposition of $p = r_1' * r_2'$. In any case, we obtain that $N(p) = 0$ for all $p \in \pi(x, z)$.

Moreover, to the complex $\widetilde{GC}(\mathbb{G})$ we can associate a *Maslov grading* and an *Alexander grading*, determined by the functions $M\colon S \to \mathbb{Z}$ and $S\colon S \to \frac{1}{2}\mathbb{Z}$. For reasons we will

see in the next section, we will in general not be concerned with these gradings, unless otherwise specified. We postpone their definitions to Section 6. It can be checked, however, that the differential ∂ decreases the Maslov grading by 1 and preserves the Alexander grading.

We can now take the homology of the chain complex $(\widetilde{\mathrm{GC}}(\mathbb{G}), \partial)$, and define

$$\widetilde{\mathrm{GH}}(\mathbb{G}) = \mathrm{H}_*(\widetilde{\mathrm{GC}}(\mathbb{G}), \partial).$$

It is shown in [11; 12] that, if $\mathbb{G}$ is a grid diagram with grid number n for the oriented link L with ℓ components, then

$$\widetilde{\mathrm{GH}}(\mathbb{G}) \cong \widehat{\mathrm{GH}}(L) \otimes V^{n-\ell},$$

where V is a 2–dimensional vector space over $\mathbb{F}_2$, spanned by one generator in (Maslov and Alexander) bigrading $(-1, -1)$ and another in bigrading $(0, 0)$, and $\widehat{\mathrm{GH}}(L)$ is a link invariant, often referred to as the *combinatorial knot Floer homology*, or *grid homology*, that is a vector space isomorphic to $\widehat{\mathrm{HFK}}(L)$. $\widetilde{\mathrm{GH}}(\mathbb{G})$ can also be denoted by $\widetilde{\mathrm{GH}}(L, n)$.

Remark 2.1 While the proof that ∂ is a differential is completely elementary, its method is very useful to what we shall prove in this paper. In general, in order to prove that a map defined by counting certain domains is a chain map, or to prove that it is a chain homotopy, we juxtapose two domains and enumerate all possible outcomes.

3 Manolescu's unoriented skein exact triangle

We now prove our main result over $\mathbb{F}_2$ in purely combinatorial terms.

Before we start our main discussion, we make a change in our notation. In the original description developed in [11; 12], the Os and Xs were used to determine the Alexander and Maslov gradings of the generators. However, given a link L_∞ in S^3 and its two resolutions L_0, L_1 at a crossing, we observe that L_∞, L_0, L_1 do not share a compatible orientation. Since we shall soon combine all three grid diagrams into one, we must forget the orientations of the links; this implies that we must also forget the distinctions between the Os and Xs, and ignore the gradings. Notice that using markers of only one type will not change the definition of $\widetilde{\mathrm{GH}}(L, n)$, since without the gradings, the definition of the chain complex $\widetilde{\mathrm{GC}}(\mathbb{G})$ associated to a grid diagram G is symmetric in the Os and the Xs. Therefore, we shall henceforth replace all Os with Xs.

With this new notation, the first two conditions for a grid diagram become the condition that there are exactly two Xs on each row and each column. We denote by $\mathbb{X}$ the set

of Xs on a grid diagram. The differential is then given by

$$\partial(\boldsymbol{x}) = \sum_{\boldsymbol{y} \in \boldsymbol{S}(\mathbb{G})} \sum_{\substack{r \in \text{Rect}^\circ(\boldsymbol{x}, \boldsymbol{y}) \\ \text{Int}(r) \cap \mathbb{X} = \varnothing}} \boldsymbol{y} \in \widetilde{\text{GC}}(\mathbb{G}).$$

To begin, we position L_∞, L_0, L_1 as in Figure 2, and make sure that their respective grid diagrams $\mathbb{G}_\infty, \mathbb{G}_0, \mathbb{G}_1$ are identical except near the crossing, as indicated in the same figure. Next, we let $C_k = \widetilde{\text{GC}}(\mathbb{G}_k)$ be the chain complex associated with $\mathbb{G}_k$, for each $k \in \{\infty, 0, 1\}$. We endow the set $\{\infty, 0, 1\}$ with an action by $\mathbb{Z}/3\mathbb{Z}$ by identifying ∞ with 2, so that $\infty + 1 = 0$ and $1 + 1 = \infty$.
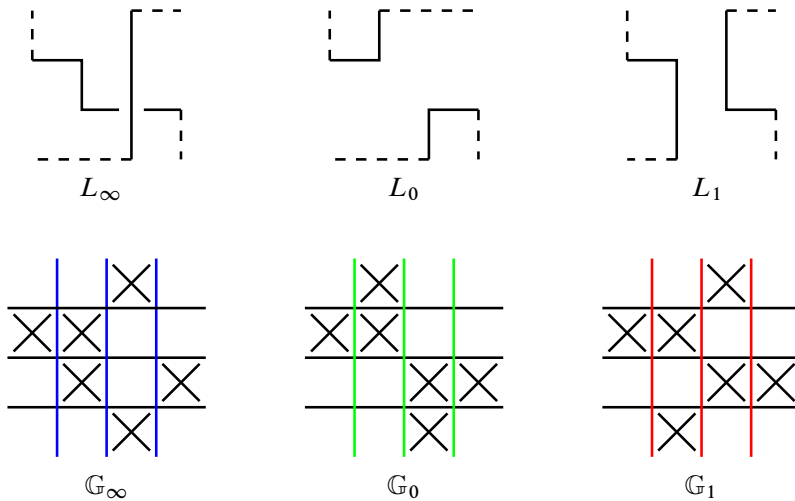

Figure 2: Grid diagrams for L_∞, L_0 and L_1 near a point

Remark 3.1 The leftmost and rightmost columns in each of the diagrams in Figure 2 do not need to be in the form displayed; the markers can be in any row in those two columns, and the proofs in this and the next section do not rely on the positions of the markers. In the figures in this section, we leave the markers there for ease of visualization. However, in Section 5, it will be necessary to have the markers exactly as they appear in Figure 2, to iterate the exact triangle.

Instead of drawing three different diagrams, we can draw $\mathbb{G}_\infty, \mathbb{G}_0, \mathbb{G}_1$ all on the same diagram, as in Figure 3. We label by β_k the vertical circle corresponding to $\mathbb{G}_k$ for each $k \in \{\infty, 0, 1\}$, as indicated. These three vertical circles, together with all the other vertical circles, divide $\mathbb{T}$ into a number of components; we let b be the unique component that is an annulus not containing any X in its interior. Also, exactly three of these components are embedded triangles not containing any X in their interior;

we let t_k be the triangle whose β_k arc is disjoint from the boundary of b. Finally, β_k and β_{k+1} intersect at exactly two points; we denote by u_k the intersection point that lies on the boundary of b, and by v_k the other intersection point. Then $u_k = b \cap t_{k+2}$ and $v_k = t_k \cap t_{k+1}$.
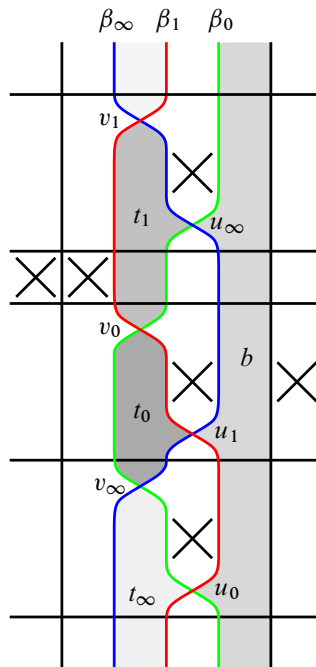

Figure 3: Combined grid diagram for L_∞, L_0 and L_1 near a point. The annulus b and the triangles t_k are shaded. The circles β_k and β_{k+1} intersect at two points; u_k are the ones on the right, and v_k are those on the left.

In this setting and over $\mathbb{F}_2$, Theorem 1.3 follows from our main proposition:

Proposition 3.2 *There exists an exact triangle*

$$\cdots \to \widetilde{GH}(\mathbb{G}_\infty; \mathbb{F}_2) \to \widetilde{GH}(\mathbb{G}_0; \mathbb{F}_2) \to \widetilde{GH}(\mathbb{G}_1; \mathbb{F}_2) \to \cdots .$$

We make use of the following lemma from homological algebra, first used by Ozsváth and Szabó [17], and used also in [9].

Lemma 3.3 *Let $\{(C_k, \partial_k)\}_{k \in \{\infty, 0, 1\}}$ be a collection of chain complexes over an arbitrary commutative ring, and let $\{f_k \colon C_k \to C_{k+1}\}_{k \in \{\infty, 0, 1\}}$ be a collection of anti-chain maps such that the following conditions are satisfied for each k:*

(1) *The composite $f_{k+1} \circ f_k \colon C_k \to C_{k+2}$ is chain-homotopic to zero, by a chain homotopy $\varphi_k \colon C_k \to C_{k+2}$:*

$$f_{k+1} \circ f_k + \partial_{k+2} \circ \varphi_k + \varphi_k \circ \partial_k = 0.$$

(2) *The map $\varphi_{k+1} \circ f_k + f_{k+2} \circ \varphi_k \colon C_k \to C_k$ is a quasi-isomorphism. (In particular, if there exists a chain homotopy $\psi_k \colon C_k \to C_k$ such that*

$$\varphi_{k+1} \circ f_k + f_{k+2} \circ \varphi_k + \partial_k \circ \psi_k + \psi_k \circ \partial_k = \mathrm{Id},$$

then this condition is satisfied.)

Then we have an exact sequence

$$\cdots \to \mathrm{H}_*(C_k) \xrightarrow{(f_k)_*} \mathrm{H}_*(C_{k+1}) \xrightarrow{(f_{k+1})_*} \mathrm{H}_*(C_{k+2}) \to \cdots .$$

We now define the chain maps $f_k \colon C_k \to C_{k+1}$ by counting pentagons and triangles.

Given $x \in S(\mathbb{G}_k)$ and $y \in S(\mathbb{G}_{k+1})$, let $\mathrm{Pent}_k(x, y)$ denote the space of embedded pentagons with the following properties. First of all, $\mathrm{Pent}_k(x, y)$ is empty unless x, y coincide at exactly $n-2$ points. An element p of $\mathrm{Pent}_k(x, y)$ is an embedded disk in $\mathbb{T}$, whose boundary consists of five arcs, each contained in horizontal or vertical circles; under the orientation induced on the boundary of p, we start at the β_k–component of x, traverse the arc of a horizontal circle, meet its corresponding component of y, proceed to an arc of a vertical circle, meet the corresponding component of x, continue through another horizontal circle, meet the component of y contained in β_{k+1}, proceed to an arc in β_{k+1}, meet the intersection point u_k of β_k and β_{k+1}, and finally, traverse an arc in β_k until we arrive back at the initial component of x. Notice that all angles here are at most straight angles. The space of empty pentagons $p \in \mathrm{Pent}_k(x, y)$ with $x \cap \mathrm{Int}(p) = \varnothing$ is denoted $\mathrm{Pent}_k^\circ(x, y)$.

Similarly, we let $\mathrm{Tri}_k(x, y)$ denote the space of embedded triangles with the following properties. $\mathrm{Tri}_k(x, y)$ is empty unless x, y coincide at exactly $n - 1$ points. An element p of $\mathrm{Tri}_k(x, y)$ is an embedded disk in $\mathbb{T}$, whose boundary consists of three arcs, each contained in horizontal or vertical circles; under the orientation induced on the boundary of p, we start at the β_k–component of x, traverse the arc of a horizontal circle, meet the component of y contained in β_{k+1}, proceed to an arc in β_{k+1}, meet the intersection point v_k of β_k and β_{k+1}, and finally traverse an arc in β_k to return to the initial component of x. Again, all the angles here are less than straight angles. It is clear that all triangles $p \in \mathrm{Tri}_k(x, y)$ satisfy $x \cap \mathrm{Int}(p) = \varnothing$. Furthermore, for any generator x, there is at most one generator y such that $\mathrm{Tri}_k(x, y)$ is not empty.

See Figure 4 for examples of elements of $\mathrm{Pent}_k^\circ(x, y)$ and $\mathrm{Tri}_k(x, y)$.
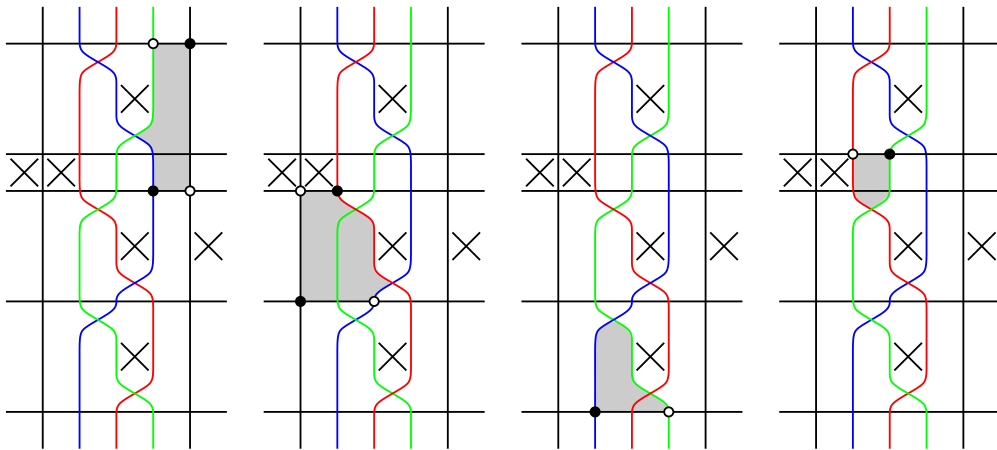
Figure 4: Two allowed pentagons in $\mathrm{Pent}_k^\circ(\boldsymbol{x}, \boldsymbol{y})$ and two allowed triangles in $\mathrm{Tri}_k(\boldsymbol{x}, \boldsymbol{y})$. The components of $\boldsymbol{x}$ are indicated by solid points, and those of $\boldsymbol{y}$ are indicated by hollow ones.

Given $\boldsymbol{x} \in \boldsymbol{S}(\mathbb{G}_k)$, we define elements of C_{k+1},

$$\mathcal{P}_k(\boldsymbol{x}) = \sum_{\boldsymbol{y} \in \boldsymbol{S}(\mathbb{G}_{k+1})} \sum_{\substack{p \in \mathrm{Pent}_k^\circ(\boldsymbol{x}, \boldsymbol{y}) \\ \mathrm{Int}(p) \cap \mathbb{X} = \varnothing}} \boldsymbol{y},$$

$$\mathcal{T}_k(\boldsymbol{x}) = \sum_{\boldsymbol{y} \in \boldsymbol{S}(\mathbb{G}_{k+1})} \sum_{\substack{p \in \mathrm{Tri}_k(\boldsymbol{x}, \boldsymbol{y}) \\ \mathrm{Int}(p) \cap \mathbb{X} = \varnothing}} \boldsymbol{y},$$

$$f_k(\boldsymbol{x}) = \mathcal{P}_k(\boldsymbol{x}) + \mathcal{T}_k(\boldsymbol{x}).$$

Lemma 3.4 *The map f_k is a chain map. In fact, $\mathcal{P}_k$ and $\mathcal{T}_k$ are both chain maps.*

Proof The proof is similar to that of [12, Lemma 3.1]. We consider domains which are obtained as the juxtaposition of a pentagon or a triangle, and a rectangle. There are a few possibilities; in particular, the polygons may be disjoint, their interiors may overlap, or they may share a common corner. If the polygons are disjoint or if their interiors overlap, the domain can be decomposed as either $r * p$ or $p * r$, and so does not contribute to $\partial_{k+1} \circ f_k + f_k \circ \partial_k$. If the polygons share a common corner, the resulting domain always has an alternate decomposition, as shown in Figure 5. In all cases, the domain can be decomposed in two ways, and makes no contribution to $\partial_{k+1} \circ f_k + f_k \circ \partial_k$. Note that each domain has exactly two decompositions, both of which are counted in $\partial_{k+1} \circ f_k + f_k \circ \partial_k$; this is not going to be the case in similar lemmas later.   □
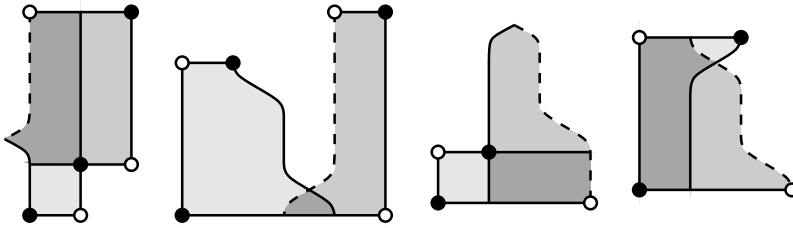
Figure 5: Two typical domains that arise as the juxtaposition of a pentagon and a rectangle, and two that arise as that of a triangle and a rectangle. The β_k curve is solid while the β_{k+1} curve is dotted.

Remark 3.5 In the proof above, every domain that arises as the juxtaposition of a triangle and a rectangle has exactly two decompositions, one contributing to $\partial_{k+1} \circ \mathcal{T}_k$ and one to $\mathcal{T}_k \circ \partial_k$. The analogous statement is not true for $\mathcal{P}_k$.

Henceforth, when considering the composition of two maps that count polygons, we shall ignore the cases where the two polygons are disjoint or have overlapping interiors, since we can always decompose the domain as either $p_1 * p_2$ or $p_2 * p_1$ in these cases.

Next, we define the chain homotopies $\varphi_k \colon C_k \to C_{k+2}$ by counting hexagons and quadrilaterals.

Given $x \in \boldsymbol{S}(\mathbb{G}_k)$ and $y \in \boldsymbol{S}(\mathbb{G}_{k+2})$, let $\mathrm{Hex}_k(x, y)$ denote the space of embedded hexagons with the following properties. First, $\mathrm{Hex}_k(x, y)$ is empty unless x and y coincide at exactly $n-2$ points. An element p of $\mathrm{Hex}_k(x, y)$ is an embedded disk in $\mathcal{T}$, whose boundary consists of six arcs, each contained in horizontal or vertical circles; under the orientation induced on the boundary of p, we start at the β_k–component of x, traverse the arc of a horizontal circle, meet its corresponding component of y, proceed to an arc of a vertical circle, meet the corresponding component of x, continue through another horizontal circle, meet the component of y contained in β_{k+2}, proceed to an arc in β_{k+2}, meet the intersection point u_{k+1} of β_{k+1} and β_{k+2}, traverse an arc in β_{k+1}, meet the intersection point u_k of β_k and β_{k+1}, and finally, traverse an arc in β_k until we arrive back at the initial component of x. All the angles here are at most straight angles. The space of empty hexagons $p \in \mathrm{Hex}_k(x, y)$ with $x \cap \mathrm{Int}(p) = \varnothing$ is denoted $\mathrm{Hex}_k^{\circ}(x, y)$.

Similarly, we let $\mathrm{Quad}_k(x, y)$ denote the space of embedded quadrilaterals with the following properties. $\mathrm{Quad}_k(x, y)$ is empty unless x, y coincide at exactly $n-1$ points. An element p of $\mathrm{Quad}_k(x, y)$ is an embedded disk in $\mathcal{T}$, whose boundary consists of four arcs, each contained in horizontal or vertical circles; under the orientation induced on the boundary of p, we start at the β_k–component of x, traverse the arc
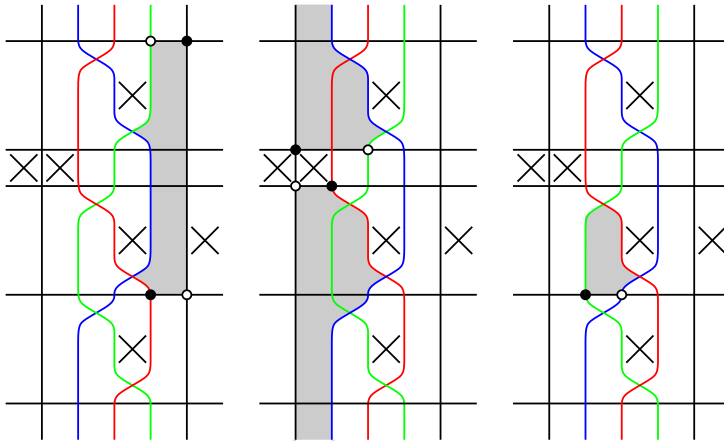
Figure 6: Two allowed hexagons in $\mathrm{Hex}_k^\circ(x, y)$ and an allowed quadrilateral in $\mathrm{Quad}_k(x, y)$. The hexagon in the middle figure is the only allowed empty hexagon that is a left domain.

of a horizontal circle, meet the component of y contained in β_{k+2}, proceed to an arc in β_{k+2}, meet the intersection point u_{k+1} of β_{k+1} and β_{k+2}, proceed to an arc in β_{k+1}, meet the intersection point v_k of β_k with β_{k+1}, and finally traverse an arc in β_k to return to the initial component of x. All the angles here are at most straight angles. It is clear that all quadrilaterals $p \in \mathrm{Tri}_k(x, y)$ satisfy $x \cap \mathrm{Int}(p) = \varnothing$.

See Figure 6 for examples of elements of $\mathrm{Hex}_k^\circ(x, y)$ and $\mathrm{Quad}_k(x, y)$.

Given $x \in S(\mathbb{G}_k)$, we define elements of C_{k+2} by

$$\mathcal{H}_k(x) = \sum_{\substack{y \in S(\mathbb{G}_{k+2})}} \sum_{\substack{p \in \mathrm{Hex}_k^\circ(x,y) \\ \mathrm{Int}(p) \cap \mathbb{X} = \varnothing}} y,$$

$$\mathcal{Q}_k(x) = \sum_{\substack{y \in S(\mathbb{G}_{k+2})}} \sum_{\substack{p \in \mathrm{Quad}_k(x,y) \\ \mathrm{Int}(p) \cap \mathbb{X} = \varnothing}} y,$$

$$\varphi_k(x) = \mathcal{H}_k(x) + \mathcal{Q}_k(x).$$

We say that a domain p is a *left domain* if $\mathrm{Int}(p) \cap \mathrm{Int}(b) = \varnothing$, and a *right domain* if $\mathrm{Int}(p) \cap \mathrm{Int}(b) \neq \varnothing$.

Lemma 3.6 *The maps f_k and φ_k satisfy condition* (1) *of Lemma 3.3.*

Proof Juxtaposing a triangle and a pentagon appearing in $\mathcal{P}_{k+1} \circ \mathcal{T}_k$, we generically obtain a composite domain that admits a unique alternative decomposition as a

quadrilateral and a rectangle, appearing in either $\partial_{k+2} \circ \mathcal{Q}_k$ or $\mathcal{Q}_k \circ \partial_k$, except for one special case, which is described in (1) below. Juxtaposing two pentagons appearing in $\mathcal{P}_{k+1} \circ \mathcal{P}_k$, we generically obtain a composite domain that admits a unique alternative decomposition as a hexagon and a rectangle, appearing in either $\partial_{k+2} \circ \mathcal{H}_k$ or $\mathcal{H}_k \circ \partial_k$, except for one special case, which is described in (3) below.

There are three special cases. We consider domains p arising from juxtapositions of:

(1)   A pentagon and a triangle appearing in $\mathcal{T}_{k+1} \circ \mathcal{P}_k$, such that the β_k–component of x does not lie on the boundary of any annular component of $\mathbb{T}$ minus the vertical circles (including β_∞, β_0, β_1). Visually, the β_k–component of x lies on the central vertical axis of the figure. The domain p can only be alternatively decomposed as the triangle t_{k+2} and a pentagon, bounded by β_k, a horizontal arc, a vertical arc, another horizontal arc and β_{k+2}, in its induced orientation. The pentagon is in the opposite orientation as one that would be counted in the map f_{k+2}, and its boundary meets only the intersection point v_{k+2}; such a pentagon is not counted in any map. The triangle t_{k+2} is not counted in any map either. Therefore, p is counted exactly once in $f_{k+1} \circ f_k + \partial_{k+2} \circ \varphi_k + \varphi_k \circ \partial_k$. However, we can replace t_{k+2} with the triangle t_k, and obtain a corresponding domain p' that also connects x to y. The new domain p' admits a unique alternative decomposition as a triangle and a pentagon, counted in $\mathcal{P}_{k+1} \circ \mathcal{T}_k$. See Figure 7(1).

(2)   A pentagon and a triangle appearing in $\mathcal{T}_{k+1} \circ \mathcal{P}_k$, such that the β_k–component of x lies on the boundary of an annular component of $\mathbb{T}$ minus the vertical circles (including β_∞, β_0, β_1). Visually, the β_k–component of x lies to the left of the central vertical axis of the figure. The domain p can only be alternatively decomposed as the triangle t_{k+2} and a pentagon, bounded by β_k, a horizontal arc, a vertical arc, another horizontal arc and β_{k+2}, in its induced orientation. The pentagon is in the opposite orientation as one that would be counted in the map f_{k+2}, and its boundary meets only the intersection point v_{k+2}; such a pentagon is not counted in any map. The triangle t_{k+2} is not counted in any map either. Therefore, p is counted exactly once in $f_{k+1} \circ f_k + \partial_{k+2} \circ \varphi_k + \varphi_k \circ \partial_k$. However, we can replace t_{k+2} with the triangle t_k, and obtain a corresponding domain p' that also connects x to y. The new domain p' admits a unique alternative decomposition as a quadrilateral and a rectangle, counted in $\partial_{k+2} \circ \mathcal{Q}_k$. See Figure 7(2).

(3)   Two triangles appearing in $\mathcal{T}_{k+1} \circ \mathcal{T}_k$. The domain p can only be alternatively decomposed as the triangle t_{k+1} and another triangle, bounded by segments of β_k, β_{k+2} and a horizontal circle in its induced orientation, and having u_{k+2} as a corner. Since neither triangle is counted in any of the maps f_k or φ_k, p is counted exactly once in $f_{k+1} \circ f_k + \partial_{k+2} \circ \varphi_k + \varphi_k \circ \partial_k$. However, we can replace t_{k+1} with the annulus b, and
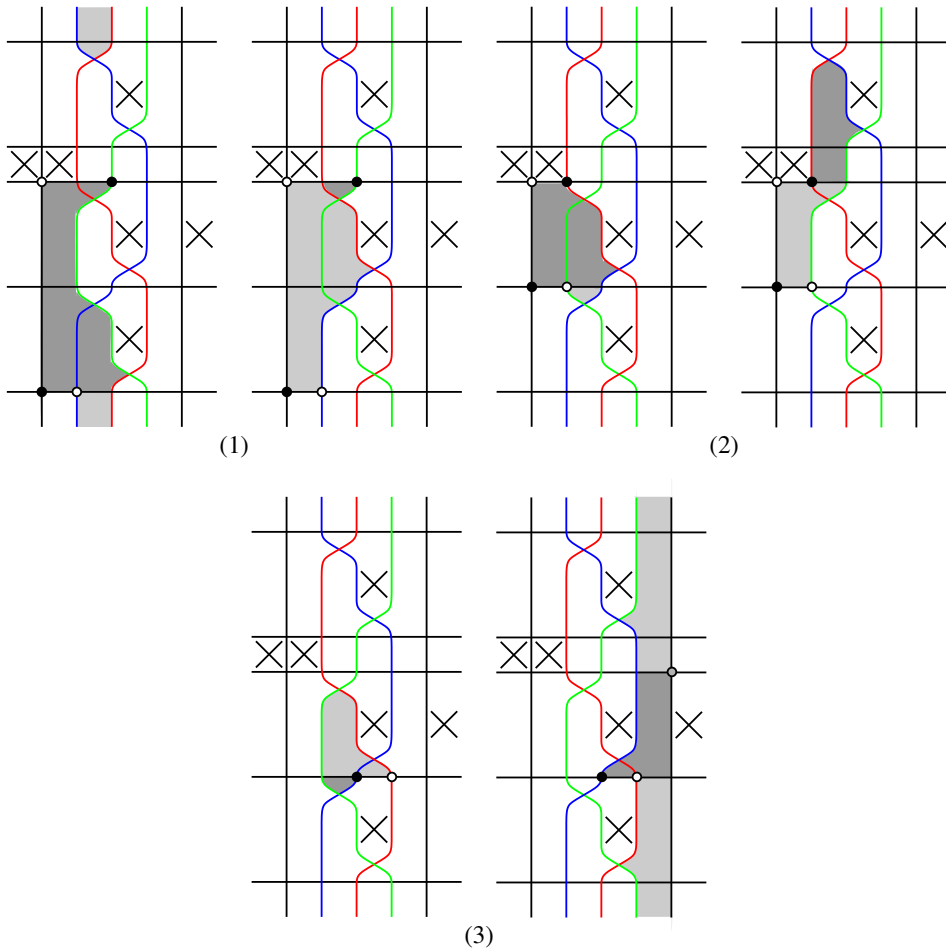
Figure 7: Three special cases. In each case, there are two domains p and p', each counted exactly once in $f_{k+1} \circ f_k + \partial_{k+2} \circ \varphi_k + \varphi_k \circ \partial_k$.

obtain a corresponding domain p' that also connects $\boldsymbol{x}$ to $\boldsymbol{y}$. The situation is similar to the special case in the proof of [12, Lemma 3.1]. Depending on the initial point $\boldsymbol{x}$, the new domain p' admits a unique alternative decomposition as two pentagons or as a hexagon and a rectangle, counted either in $\mathcal{P}_{k+1} \circ \mathcal{P}_k$, in $\partial_{k+2} \circ \mathcal{H}_k$, or in $\mathcal{H}_k \circ \partial_k$. See Figure 7(3).

Finally, the remaining terms in $\partial_{k+2} \circ \mathcal{Q}_k$ cancel with terms in $\mathcal{Q}_k \circ \partial_k$, and the remaining terms in $\partial_{k+2} \circ \mathcal{H}_k$ cancel with terms in $\mathcal{H}_k \circ \partial_k$. Table 1 summarizes how the terms cancel each other.   □

We now define the chain homotopy $\psi_k \colon C_k \to C_k$ by counting heptagons.

	term in	position	cancels with term in	special case
$f_{k+1} \circ f_k$	$\mathcal{P}_{k+1} \circ \mathcal{P}_k$	left, right ($\not\supset b$)	$\partial_{k+2} \circ \mathcal{H}_k$ or $\mathcal{H}_k \circ \partial_k$	
		right ($\supset b$)	$\mathcal{T}_{k+1} \circ \mathcal{T}_k$	(3)
	$\mathcal{T}_{k+1} \circ \mathcal{P}_k$	left (central x)	$\mathcal{P}_{k+1} \circ \mathcal{T}_k$	(1)
		left (left x)	$\partial_{k+2} \circ \mathcal{Q}_k$	(2)
	$\mathcal{P}_{k+1} \circ \mathcal{T}_k$	left (central y)	$\mathcal{Q}_k \circ \partial_k$	
		left (otherwise)	$\mathcal{T}_{k+1} \circ \mathcal{P}_k$	(1)
		right	$\partial_{k+2} \circ \mathcal{Q}_k$	
	$\mathcal{T}_{k+1} \circ \mathcal{T}_k$	left	$\mathcal{P}_{k+1} \circ \mathcal{P}_k, \partial_{k+2} \circ \mathcal{H}_k$ or $\mathcal{H}_k \circ \partial_k$	(3)
$\partial_{k+2} \circ \varphi_k$	$\partial_{k+2} \circ \mathcal{H}_k$	left	$\mathcal{P}_{k+1} \circ \mathcal{P}_k$	
		right ($\not\supset b$)	$\mathcal{P}_{k+1} \circ \mathcal{P}_k$ or $\mathcal{H}_k \circ \partial_k$	
		right ($\supset b$)	$\mathcal{T}_{k+1} \circ \mathcal{T}_k$	(3)
	$\partial_{k+2} \circ \mathcal{Q}_k$	left (central y)	$\mathcal{Q}_k \circ \partial_k$	
		left (otherwise)	$\mathcal{T}_{k+1} \circ \mathcal{P}_k$	(2)
		right	$\mathcal{P}_{k+1} \circ \mathcal{T}_k$ or $\mathcal{Q}_k \circ \partial_k$	
$\varphi_k \circ \partial_k$	$\mathcal{H}_k \circ \partial_k$	left	$\mathcal{P}_{k+1} \circ \mathcal{P}_k$	
		right ($\not\supset b$)	$\mathcal{P}_{k+1} \circ \mathcal{P}_k$ or $\partial_{k+2} \circ \mathcal{H}_k$	
		right ($\supset b$)	$\mathcal{T}_{k+1} \circ \mathcal{T}_k$	(3)
	$\mathcal{Q}_k \circ \partial_k$	left	$\mathcal{P}_{k+1} \circ \mathcal{T}_k$ or $\partial_{k+2} \circ \mathcal{Q}_k$	
		right	$\partial_{k+2} \circ \mathcal{Q}_k$	

Table 1: This table shows how the terms cancel each other in Lemma 3.6. A left domain is indicated as "(central x)" if the β_k–component of x lies on the central vertical axis of the figure, and "(left x)" if it lies to the left of this axis; similarly for y. A right domain is indicated as "($\supset b$)" if $\mathrm{Int}(p) \supset \mathrm{Int}(b)$, and "($\not\supset b$)" otherwise. The special cases are shown in Figure 7.

Given $x \in S(\mathbb{G}_k)$ and $y \in S(\mathbb{G}_{k+2})$, let $\mathrm{Hept}_k(x, y)$ denote the space of embedded heptagons. First of all, $\mathrm{Hept}_k(x, y)$ is empty unless x, y coincide at exactly $n - 2$ points. An element p of $\mathrm{Hept}_k(x, y)$ is an embedded disk in $\mathbb{T}$, whose boundary consists of seven arcs, each contained in horizontal or vertical circles; under the orientation induced on the boundary of p, we start at the β_k–component of x, traverse the arc of a horizontal circle, meet its corresponding component of y, proceed to an arc of a vertical circle, meet the corresponding component of x, continue through another horizontal circle, meet the component of y contained in β_k, proceed to an arc in β_k, meet the intersection point u_{k+2} of β_k and β_{k+2}, proceed to an arc in β_{k+2},
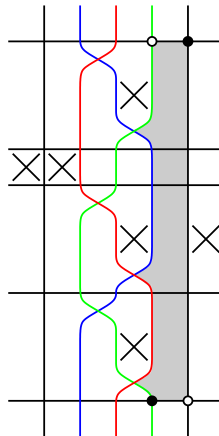
Figure 8: An allowed heptagon in $\text{Hept}_k^\circ(\boldsymbol{x}, \boldsymbol{y})$. Note that allowed heptagons are necessarily right domains.

meet the intersection point u_{k+1} of β_{k+1} and β_{k+2}, traverse an arc in β_{k+1}, meet the intersection point u_k of β_k and β_{k+1}, and finally, traverse an arc in β_k until we arrive back at the initial component of $\boldsymbol{x}$. All the angles here are again at most straight angles. The space of empty heptagons $p \in \text{Hept}_k(\boldsymbol{x}, \boldsymbol{y})$ with $\boldsymbol{x} \cap \text{Int}(p) = \varnothing$ is denoted $\text{Hept}_k^\circ(\boldsymbol{x}, \boldsymbol{y})$.

See Figure 8 for an example of an element of $\text{Hept}_k^\circ(x, y)$.

Given $\boldsymbol{x} \in \boldsymbol{S}(\mathbb{G}_k)$, we define

$$\psi_k(\boldsymbol{x}) = \mathcal{K}_k(\boldsymbol{x}) = \sum_{\boldsymbol{y} \in \boldsymbol{S}(\mathbb{G}_k)} \sum_{\substack{p \in \text{Hept}_k^\circ(\boldsymbol{x}, \boldsymbol{y}) \\ \text{Int}(p) \cap \mathbb{X} = \varnothing}} \boldsymbol{y} \in C_k.$$

Lemma 3.7 *We have*

$$\varphi_{k+1} \circ f_k + f_{k+2} \circ \varphi_k + \partial_k \circ \psi_k + \psi_k \circ \partial_k = \text{Id},$$

so that the maps f_k and φ_k satisfy condition (2) of Lemma 3.3.

Proof First, we see that juxtaposing either a triangle and a hexagon, or a pentagon and a quadrilateral, does not contribute to $\varphi_{k+1} \circ f_k + f_{k+2} \circ \varphi_k$. In other words, we first claim that $\mathcal{P}_{k+2} \circ \mathcal{Q}_k + \mathcal{Q}_{k+1} \circ \mathcal{P}_k + \mathcal{H}_{k+1} \circ \mathcal{T}_k + \mathcal{T}_{k+2} \circ \mathcal{H}_k = 0$.

There are exactly four cases. We consider domains p formed by juxtaposing:

(1) A quadrilateral and a pentagon appearing in $\mathcal{P}_{k+2} \circ \mathcal{Q}_k$, such that p is a right domain. In this case, p admits a unique alternative decomposition as a triangle and a hexagon appearing in $\mathcal{H}_{k+1} \circ \mathcal{T}_k$. See Figure 9(1).
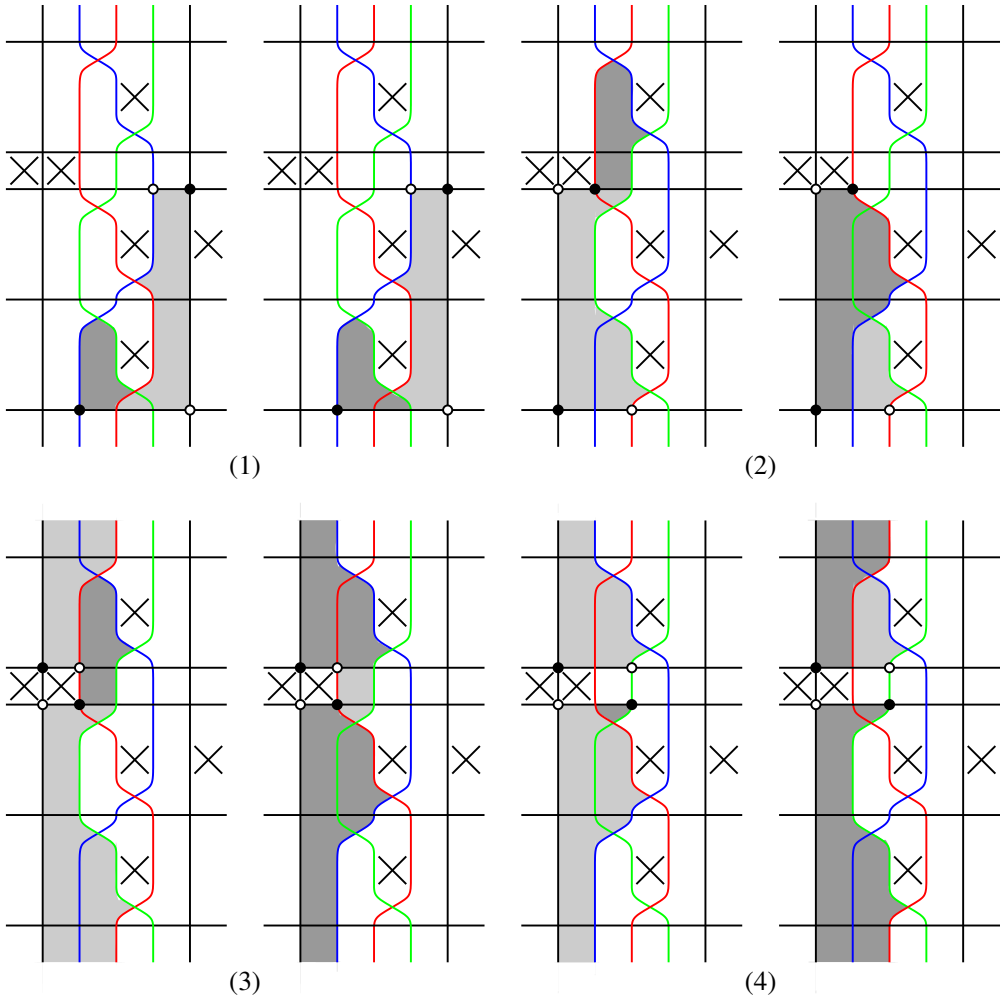
Figure 9: The four cases when juxtaposing a triangle and a hexagon, or a pentagon and a quadrilateral. All terms that arise cancel out with each other.

(2)   A quadrilateral and a pentagon appearing in $\mathcal{P}_{k+2} \circ \mathcal{Q}_k$, such that p is a left domain with height less than n. Only this decomposition of p is counted. However, we can replace the triangle t_k inside p by the triangle t_{k+2}, and obtain a corresponding domain p' that can be uniquely decomposed as a pentagon and a quadrilateral appearing in $\mathcal{Q}_{k+1} \circ \mathcal{P}_k$. See Figure 9(2).

(3)   A quadrilateral and a pentagon appearing in $\mathcal{P}_{k+2} \circ \mathcal{Q}_k$, such that p is a right domain with height n. This is in fact only possible when $k = 1$. Only this decomposition of p is counted. However, p contains the triangles t_k and t_{k+1}; we can replace t_{k+1}
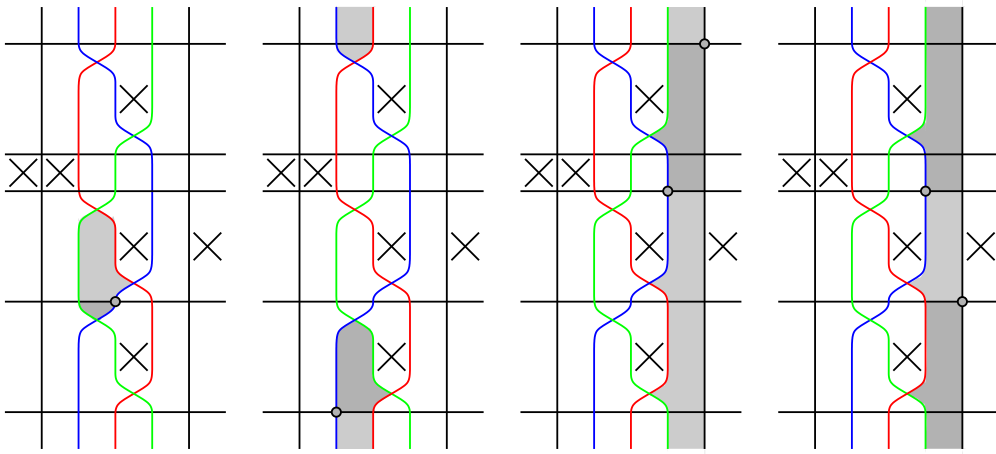
Figure 10: Decomposing the identity map

by the triangle t_{k+2}, and obtain a corresponding domain p' that can be uniquely decomposed as a hexagon and a triangle appearing in $\mathcal{T}_{k+2} \circ \mathcal{H}_k$. See Figure 9(3).

The astute reader may find it strange that in this particular case, in p the triangle t_k is "attached" to the top of the rest of the domain, whereas in p' it is "attached" to the bottom. One way to convince oneself of the validity of the procedure of obtaining p' from p, is to think of it as first replacing t_k by t_{k+2}, and then replacing t_{k+1} by t_k.

(4)   A triangle and a hexagon appearing in $\mathcal{H}_{k+1} \circ \mathcal{T}_k$, such that p is a left domain. This is only possible when $k = 0$. Only this decomposition of p is counted. However, we can replace the triangle t_k inside p by the triangle t_{k+2}, and obtain a corresponding domain p' that can be uniquely decomposed as a pentagon and a quadrilateral appearing in $\mathcal{Q}_{k+1} \circ \mathcal{P}_k$. See Figure 9(4).

Juxtaposing a pentagon and a hexagon appearing in $\mathcal{H}_{k+1} \circ \mathcal{P}_k$ or $\mathcal{P}_{k+2} \circ \mathcal{H}_k$, we generically obtain a composite domain that admits a unique alternative decomposition as a heptagon and a rectangle, appearing in $\partial_k \circ \mathcal{K}_k$ or $\mathcal{K}_k \circ \partial_k$, except for one special case discussed below.

Depending on the initial point $\boldsymbol{x}$, there exists exactly one domain p connecting $\boldsymbol{x}$ to itself that admits a unique decomposition, either as a triangle and a quadrilateral in $\mathcal{Q}_{k+1} \circ \mathcal{T}_k$ (in which case p is the triangle t_{k+1}), as a quadrilateral and a triangle in $\mathcal{T}_{k+2} \circ \mathcal{Q}_k$ (p is the triangle t_k), as a pentagon and a hexagon appearing in $\mathcal{H}_{k+1} \circ \mathcal{P}_k$ or $\mathcal{P}_{k+2} \circ \mathcal{H}_k$ (p is the annulus b), or as a rectangle and a heptagon appearing in $\mathcal{K}_k \circ \partial_k$ or $\partial_k \circ \mathcal{K}_k$ (p is again the annulus b). Of course, in this case, the identity map is counted once. See Figure 10.

	term in	position	cancels with term in	special case
$\varphi_{k+1} \circ f_k$	$\mathcal{H}_{k+1} \circ \mathcal{P}_k$	right ($\neq b$)	$\partial_k \circ \mathcal{K}_k$ or $\mathcal{K}_k \circ \partial_k$	
		right ($= b$)	Id	
	$\mathcal{Q}_{k+1} \circ \mathcal{P}_k$	left (ht. $< n-1$)	$\mathcal{P}_{k+2} \circ \mathcal{Q}_k$	(2)
		left (ht. $= n-1$)	$\mathcal{H}_{k+1} \circ \mathcal{T}_k$	(4)
	$\mathcal{H}_{k+1} \circ \mathcal{T}_k$	left	$\mathcal{Q}_{k+1} \circ \mathcal{P}_k$	(4)
		right	$\mathcal{P}_{k+2} \circ \mathcal{Q}_k$	(1)
	$\mathcal{Q}_{k+1} \circ \mathcal{T}_k$	left	Id	
$f_{k+2} \circ \varphi_k$	$\mathcal{P}_{k+2} \circ \mathcal{H}_k$	right ($\neq b$)	$\partial_k \circ \mathcal{K}_k$ or $\mathcal{K}_k \circ \partial_k$	
		right ($= b$)	Id	
	$\mathcal{T}_{k+2} \circ \mathcal{H}_k$	left	$\mathcal{P}_{k+2} \circ \mathcal{Q}_k$	(3)
	$\mathcal{P}_{k+2} \circ \mathcal{Q}_k$	left (ht. $< n$)	$\mathcal{Q}_{k+1} \circ \mathcal{P}_k$	(2)
		left (ht. $= n$)	$\mathcal{T}_{k+1} \circ \mathcal{H}_k$	(3)
		right	$\mathcal{H}_{k+1} \circ \mathcal{T}_k$	(1)
	$\mathcal{T}_{k+2} \circ \mathcal{Q}_k$	left	Id	
$\partial_k \circ \psi_k$	$\partial_k \circ \mathcal{K}_k$	right	$\mathcal{H}_{k+1} \circ \mathcal{P}_k, \mathcal{P}_{k+2} \circ \mathcal{H}_k,$ $\mathcal{K}_k \circ \partial_k$ or Id	
$\psi_k \circ \partial_k$	$\mathcal{K}_k \circ \partial_k$	right	$\mathcal{H}_{k+1} \circ \mathcal{P}_k, \mathcal{P}_{k+2} \circ \mathcal{H}_k,$ $\partial_k \circ \mathcal{K}_k$ or Id	
Id		n/a	$\mathcal{H}_{k+1} \circ \mathcal{P}_k, \mathcal{P}_{k+2} \circ \mathcal{H}_k,$ $\partial_k \circ \mathcal{K}_k, \mathcal{K}_k \circ \partial_k,$ $\mathcal{Q}_{k+1} \circ \mathcal{T}_k$ or $\mathcal{T}_{k+2} \circ \mathcal{Q}_k$	

Table 2: This table shows how the terms cancel each other in Lemma 3.7.
The special cases are shown in Figure 9.

Finally, the remaining terms in $\partial_k \circ \mathcal{K}_k$ cancel with terms in $\mathcal{K}_k \circ \partial_k$. Table 2 summarizes how the terms above cancel each other.   □

The proof of Proposition 3.2 is completed by combining Lemmas 3.3, 3.4, 3.6 and 3.7.

4 Signs

Sign refinements are given by Manolescu, Ozsváth, Szabó and Thurston [12] to extend the definition of combinatorial knot Floer homology to one with coefficients in $\mathbb{Z}$.

In this section, we shall likewise assign sign refinements to our maps, to prove the analogous statement of Proposition 3.2 with coefficients in $\mathbb{Z}$.

Given a grid diagram, we denote by Rect° the union of $\mathrm{Rect}^\circ(x, y)$ for all x, y. We follow [12] and adopt the following definition.

Definition 4.1 A *true sign assignment*, or simply a *sign assignment*, is a function

$$\mathcal{S}: \mathrm{Rect}^\circ \to \{\pm 1\}$$

with the following properties:

(1) For any four distinct $r_1, r_2, r_1', r_2' \in \mathrm{Rect}^\circ$ with $r_1 * r_2 = r_1' * r_2'$, we have

$$\mathcal{S}(r_1) \cdot \mathcal{S}(r_2) = -\mathcal{S}(r_1') \cdot \mathcal{S}(r_2').$$

(2) For $r_1, r_2 \in \mathrm{Rect}^\circ$ such that $r_1 * r_2$ is a vertical annulus, we have

$$\mathcal{S}(r_1) \cdot \mathcal{S}(r_2) = -1.$$

(3) For $r_1, r_2 \in \mathrm{Rect}^\circ$ such that $r_1 * r_2$ is a horizontal annulus, we have

$$\mathcal{S}(r_1) \cdot \mathcal{S}(r_2) = +1.$$

Theorem 4.2 (Manolescu, Ozsváth, Szabó and Thurston) *There exists a sign assignment as defined in Definition 4.1. Moreover, this sign assignment is essentially unique: if $\mathcal{S}_1$ and $\mathcal{S}_2$ are two sign assignments, then there is a function $g: \boldsymbol{S}(\mathbb{G}) \to \{\pm 1\}$ such that $\mathcal{S}_2(r) = g(x) \cdot g(y) \cdot \mathcal{S}_1(r)$ for all $r \in \mathrm{Rect}^\circ(x, y)$.*

Remark 4.3 In the construction of a sign assignment in [12], the sign of a rectangle does not depend on the positions of the Os and Xs of the diagram. We can view each generator x as a permutation σ_x: if the component of x on the ith horizontal circle lies on the $s(i)^{\mathrm{th}}$ vertical circle, then we let σ_x be $(s(1)\, s(2) \cdots s(n))$. Then the sign of a rectangle in $\mathrm{Rect}^\circ(x, y)$ depends only on σ_x and σ_y.

The sign assignment from Theorem 4.2 is then used in [12] to construct a chain complex over $\mathbb{Z}$ as follows. The complex $\widetilde{\mathrm{GC}}(\mathbb{G}) = \widetilde{\mathrm{GC}}(\mathbb{G}; \mathbb{Z})$ is the free $\mathbb{Z}$–module generated by elements of $\boldsymbol{S}(\mathbb{G})$. Fixing a sign assignment $\mathcal{S}$, the complex $\widetilde{\mathrm{GC}}(\mathbb{G})$ is endowed with the endomorphism $\partial_{\mathcal{S}}: \widetilde{\mathrm{GC}}(\mathbb{G}) \to \widetilde{\mathrm{GC}}(\mathbb{G})$, defined by

$$\partial_{\mathcal{S}}(x) = \sum_{y \in \boldsymbol{S}(\mathbb{G})} \sum_{\substack{r \in \mathrm{Rect}^\circ(x,y) \\ \mathrm{Int}(r) \cap \mathbb{X} = \varnothing}} \mathcal{S}(r) \cdot y \in \widetilde{\mathrm{GC}}(\mathbb{G}).$$

One can then see that $(\widetilde{\mathrm{GC}}(\mathbb{G}), \partial_{\mathcal{S}})$ is a chain complex. Indeed, the terms in $\partial_{\mathcal{S}} \circ \partial_{\mathcal{S}}(x)$ can be paired off as before, by the axioms defining $\mathcal{S}$. Moreover, given $\mathcal{S}_1$ and $\mathcal{S}_2$, the

map $\Phi\colon (\widetilde{GC}(\mathbb{G}), \partial_{\mathcal{S}_1}) \to (\widetilde{GC}(\mathbb{G}), \partial_{\mathcal{S}_2})$, defined by

$$\Phi(\boldsymbol{x}) = g(\boldsymbol{x}) \cdot \boldsymbol{x},$$

gives an isomorphism of the two chain complexes. Again, one can take the homology of the chain complex $(\widetilde{GC}(\mathbb{G}), \partial_{\mathcal{S}})$, and define

$$\widetilde{GH}(\mathbb{G}) = H_*(\widetilde{GC}(\mathbb{G}), \partial_{\mathcal{S}}).$$

It is shown in [12] that

$$\widetilde{GH}(\mathbb{G}) \cong \widehat{GH}(\mathbb{G}) \otimes V^{n-\ell}$$

for some $\mathbb{Z}$–module $\widehat{GH}(\mathbb{G})$ that is a link invariant, where V is a rank 2 free module over $\mathbb{Z}$, spanned by one generator in bigrading $(-1, -1)$ and another in bigrading $(0, 0)$. The link invariant $\widehat{GH}(\mathbb{G})$, also denoted by $\widehat{GH}(L)$, is shown by Sarkar [21] to be isomorphic to $\widehat{HFK}(L, \mathfrak{o})$ for some *orientation system* $\mathfrak{o}$ of the link L.

We are now ready to turn to the proof of the analogous statement of Proposition 3.2, with signs.

Proposition 4.4 *There exists an exact triangle*

$$\cdots \to \widetilde{GH}(\mathbb{G}_\infty; \mathbb{Z}) \to \widetilde{GH}(\mathbb{G}_0; \mathbb{Z}) \to \widetilde{GH}(\mathbb{G}_1; \mathbb{Z}) \to \cdots.$$

Our proof is reminiscent of that in [12, Section 4]. We adopt the strategy from Section 3; to do so, we must specify the signs used in defining our various chain maps and chain homotopies, and check that they indeed satisfy Lemma 3.3.

We begin by considering pentagons. First, we define the notion of a *corresponding generator*. For each $\boldsymbol{x} \in C_k$, there exist exactly one $\boldsymbol{x}' \in C_{k+1}$ and one $\boldsymbol{x}'' \in C_{k+2}$ that are canonically closest to $\boldsymbol{x}$; we require that $\boldsymbol{x}$, $\boldsymbol{x}'$ and $\boldsymbol{x}''$ coincide everywhere except on the β curves, and $\boldsymbol{x}'$ and $\boldsymbol{x}''$ are obtained from $\boldsymbol{x}$ by sliding the β_k–component horizontally to the β_{k+1} and β_{k+2} curves respectively. We define the maps $c_k^+\colon C_k \to C_{k+1}$ and $c_k^-\colon C_k \to C_{k+2}$ by

$$c_k^+(\boldsymbol{x}) = \boldsymbol{x}' \quad \text{and} \quad c_k^-(\boldsymbol{x}) = \boldsymbol{x}''.$$

We can now define the straightening maps

$$d_k^{\mathcal{P}}\colon \text{Pent}_k^\circ(\boldsymbol{x}, \boldsymbol{y}) \to \text{Rect}_k^\circ(\boldsymbol{x}, c_k^-(\boldsymbol{y})), \quad e_k^{\mathcal{P}}\colon \text{Pent}_k^\circ(\boldsymbol{x}, \boldsymbol{y}) \to \text{Rect}_{k+1}^\circ(c_k^+(\boldsymbol{x}), \boldsymbol{y}),$$

as follows. Given $p \in \text{Pent}_k^\circ(\boldsymbol{x}, \boldsymbol{y})$, we obtain $d_k^{\mathcal{P}}(p)$ by sliding the β_{k+1}–component of $\boldsymbol{y}$ back to the β_k curve, thereby postcomposing p with a triangle; similarly,

we obtain $e_k^{\mathcal{P}}(p)$ by sliding the β_k–component of $\boldsymbol{x}$ to the β_{k+1} curve, thereby precomposing p with another triangle. Notice that by Remark 4.3, we have

$$\mathcal{S}(d_k^{\mathcal{P}}(p)) = \mathcal{S}(e_k^{\mathcal{P}}(p)).$$

We now define

$$\mathcal{P}_k(\boldsymbol{x}) = \sum_{\boldsymbol{y} \in \boldsymbol{S}(\mathbb{G}_{k+1})} \sum_{\substack{p \in \mathrm{Pent}_k^\circ(\boldsymbol{x},\boldsymbol{y}) \\ \mathrm{Int}(p) \cap \mathbb{X} = \varnothing}} \epsilon_k^{\mathcal{P}}(p) \cdot \boldsymbol{y} \ \in C_{k+1},$$

where

$$\epsilon_k^{\mathcal{P}}(p) = \begin{cases} \mathcal{S}(d_k^{\mathcal{P}}(p)) & \text{if } p \text{ is a left pentagon,} \\ -\mathcal{S}(d_k^{\mathcal{P}}(p)) & \text{if } p \text{ is a right pentagon.} \end{cases}$$

Turning to triangles, we again view generators as permutations. The signature $\mathrm{sgn}(\boldsymbol{x})$ of a generator $\boldsymbol{x}$ is defined to be the signature $\mathrm{sgn}(\sigma_{\boldsymbol{x}})$ of the corresponding permutation. Then we define

$$\mathcal{T}_k(\boldsymbol{x}) = \sum_{\boldsymbol{y} \in \boldsymbol{S}(\mathbb{G}_{k+1})} \sum_{\substack{p \in \mathrm{Tri}_k(\boldsymbol{x},\boldsymbol{y}) \\ \mathrm{Int}(p) \cap \mathbb{X} = \varnothing}} \epsilon_k^{\mathcal{T}}(p) \cdot \boldsymbol{y} \ \in C_{k+1},$$

where

$$\epsilon_k^{\mathcal{T}}(p) = \mathrm{sgn}(\boldsymbol{x}).$$

Finally, we define

$$f_k(\boldsymbol{x}) = \mathcal{P}_k(\boldsymbol{x}) + \mathcal{T}_k(\boldsymbol{x}) \in C_{k+1}.$$

Lemma 4.5 *The map f_k is an anti-chain map. In fact, $\mathcal{P}_k$ and $\mathcal{T}_k$ are both anti-chain maps.*

Proof The proof follows from the proof of Lemma 3.4. We first consider the juxtaposition of a pentagon and a rectangle. If the two polygons are disjoint or have overlapping interiors, then the domain can be decomposed as either $r * p$ or $p' * r'$; then by property (1) of Definition 4.1, $\mathcal{S}(r) \cdot \mathcal{S}(d_k^{\mathcal{P}}(p)) = -\mathcal{S}(d_k^{\mathcal{P}}(p')) \cdot \mathcal{S}(r')$, and consequently $\mathcal{S}(r) \cdot \epsilon_k^{\mathcal{P}}(p) = -\epsilon_k^{\mathcal{P}}(p') \cdot \mathcal{S}(r')$. If the two polygons share a corner, then the domain can be decomposed in two ways; straightening the pentagons (with either $d_k^{\mathcal{P}}$ or $e_k^{\mathcal{P}}$) and using property (1) of Definition 4.1, we again see that the terms cancel.

Consider now the juxtaposition of a triangle p and a rectangle r. Notice first that the differential ∂ always changes the signature of a generator; this means that $\mathcal{S}(r) \cdot \epsilon_k^{\mathcal{T}}(p) = -\epsilon_k^{\mathcal{T}}(p') \cdot \mathcal{S}(r')$. By Remark 3.5, such a domain can always be decomposed in two ways, one contributing to $\partial_{k+1} \circ \mathcal{T}_k$, and one to $\mathcal{T}_k \circ \partial_k$; moreover, the two rectangles involved correspond to the same permutation, and so in fact have the same sign. $\qquad\square$

We similarly define the straightening maps

$$d_k^{\mathcal{H}} \colon \operatorname{Hex}_k^{\circ}(\boldsymbol{x}, \boldsymbol{y}) \to \operatorname{Rect}_k^{\circ}(\boldsymbol{x}, c_k^{+}(\boldsymbol{y})), \quad e_k^{\mathcal{H}} \colon \operatorname{Hex}_k^{\circ}(\boldsymbol{x}, \boldsymbol{y}) \to \operatorname{Rect}_{k+2}^{\circ}(c_k^{-}(\boldsymbol{x}), \boldsymbol{y})$$

by sliding the appropriate component, and again notice that $\mathcal{S}(d_k^{\mathcal{H}}(p)) = \mathcal{S}(e_k^{\mathcal{H}}(p))$. We define

$$\mathcal{H}_k(\boldsymbol{x}) = \sum_{\boldsymbol{y} \in \boldsymbol{S}(\mathbb{G}_{k+2})} \sum_{\substack{p \in \operatorname{Hex}_k^{\circ}(\boldsymbol{x}, \boldsymbol{y}) \\ \operatorname{Int}(p) \cap \mathbb{X} = \varnothing}} \epsilon_k^{\mathcal{H}}(p) \cdot \boldsymbol{y} \ \in C_{k+2},$$

where

$$\epsilon_k^{\mathcal{H}}(p) = \mathcal{S}(d_k^{\mathcal{H}}(p)).$$

For quadrilaterals,

$$\mathcal{Q}_k(\boldsymbol{x}) = \sum_{\boldsymbol{y} \in \boldsymbol{S}(\mathbb{G}_{k+2})} \sum_{\substack{p \in \operatorname{Quad}_k(\boldsymbol{x}, \boldsymbol{y}) \\ \operatorname{Int}(p) \cap \mathbb{X} = \varnothing}} \epsilon_k^{\mathcal{Q}}(p) \cdot \boldsymbol{y} \ \in C_{k+2},$$

where

$$\epsilon_k^{\mathcal{Q}}(p) = \operatorname{sgn}(\boldsymbol{x}).$$

Lemma 4.6 *The maps f_k and φ_k satisfy condition* (1) *of Lemma 3.3.*

Proof Again the proof follows from that of Lemma 3.6. We say that a domain p is *rectangle-like* if it is an allowed rectangle, pentagon, hexagon or heptagon, and we write $p \in \operatorname{RL}$; we say that it is *triangle-like* if it is an allowed triangle or quadrilateral, and we write $p \in \operatorname{TL}$. We say a domain p is *Type I* if $p \in \operatorname{RL} * \operatorname{RL}$, *Type II* if $p \in \operatorname{RL} * \operatorname{TL}$, *Type III* if $p \in \operatorname{TL} * \operatorname{RL}$, and *Type IV* if $p \in \operatorname{TL} * \operatorname{TL}$. (Recall that $*$ and $\circ$ compose in the opposite order, so a term in $\mathcal{P}_{k+1} \circ \mathcal{T}_k$ is in $\operatorname{TL} * \operatorname{RL}$.) Refer to Table 1. Typically, a domain can be decomposed in two ways; usually, it fits into one of these cases:

(1) **Both decompositions are Type I** In this case, we see that the terms cancel out by straightening the polygons and applying property (1) of Definition 4.1.

(2) **One decomposition is Type II and one is Type III** The domain is a left domain. In this case, the terms cancel out because the two rectangle-like polygons have the same sign, but the two triangle-like polygons have opposite signs.

(3) **Both decompositions are Type III** The domain is a right domain. In this case, the two triangle-like polygons have the same sign. However, the two rectangle-like polygons are both right domains, and one is a rectangle while the other is a pentagon. Since right pentagons have opposite signs as the straightened rectangles, the two rectangle-like polygons are of opposite sign.

The only special cases are those that involve two different domains, which are exactly the special cases in Lemma 3.6.

(1) In this case, the two pentagons have the same sign, but the two triangles have opposite signs.

(2) In this case, the rectangle and the pentagon have the same sign, but the triangle and the quadrilateral have opposite signs.

(3) In one domain, the two triangles have the same sign, and so their composite is positive; in the other domain, the composite of the straightened rectangles is a vertical annulus, and so is negative by property (2) of Definition 4.1.

Since there are no other cases, our proof is complete. □

For heptagons, there is only one straightening map $d_k^{\mathcal{K}} \colon \mathrm{Hept}_k^\circ(\boldsymbol{x}, \boldsymbol{y}) \to \mathrm{Rect}_k^\circ(\boldsymbol{x}, \boldsymbol{y})$. Since the only allowed heptagons are right heptagons, putting $\epsilon_k^{\mathcal{K}}(p) = -\mathcal{S}(d_k^{\mathcal{K}}(p))$ we define

$$\mathcal{K}_k(\boldsymbol{x}) = \sum_{\boldsymbol{y} \in \boldsymbol{S}(\mathbb{G}_k)} \sum_{\substack{p \in \mathrm{Hept}_k^\circ(\boldsymbol{x}, \boldsymbol{y}) \\ \mathrm{Int}(p) \cap \mathbb{X} = \varnothing}} \epsilon_k^{\mathcal{K}}(p) \cdot \boldsymbol{y} \ \in C_k.$$

Lemma 4.7 *We have*

$$\varphi_{k+1} \circ f_k + f_{k+2} \circ \varphi_k + \partial_k \circ \psi_k + \psi_k \circ \partial_k = \mathrm{Id},$$

so that the maps f_k and φ_k satisfy condition (2) of Lemma 3.3.

Proof The typical cases are as in the proof of Lemma 4.6. We check the special cases in Lemma 3.7.

(1) This is actually a typical case; the two decompositions of the domain are both Type III.

(2) In this case, the pentagons have the same sign, but the quadrilaterals have opposite signs.

(3) In this case, the pentagon and the hexagon have the same sign, but the triangle and the quadrilateral have opposite signs.

(4) Also in this case, the pentagon and the hexagon have the same sign, but the triangle and the quadrilateral have opposite signs.

We now check the decomposition of the identity map. If it is decomposed as a triangle and a quadrilateral, we see that they are of the same sign, and so we obtain a positive domain. If it is decomposed as a pentagon and a hexagon, we see that the composite of the straightened rectangles is negative by property (2) of Definition 4.1, but the right pentagon and its straightening have opposite signs; this means that the overall domain is also positive. □

The proof of Proposition 4.4 is completed by combining Lemmas 3.3, 4.5, 4.6 and 4.7.

5 Iteration of the skein exact triangle

In this section, we will work only over $\mathbb{F}_2$. Let $\mathbb{G}_\infty$, $\mathbb{G}_0$, $\mathbb{G}_1$ be grid diagrams that are identical except near a point, as indicated in Figure 2. In Section 3, we constructed the maps $f_k \colon \widetilde{GC}(\mathbb{G}_k) \to \widetilde{GC}(\mathbb{G}_{k+1})$ and $\varphi_k \colon \widetilde{GC}(\mathbb{G}_k) \to \widetilde{GC}(\mathbb{G}_{k+2})$ that satisfy Lemma 3.3. Now Lemma 3.3 and the five lemma together imply that $\widetilde{GC}(\mathbb{G}_\infty)$ is quasi-isomorphic to the mapping cone of $f_0 \colon \widetilde{GC}(\mathbb{G}_0) \to \widetilde{GC}(\mathbb{G}_1)$ (see [17, Lemma 4.2]), where the quasi-isomorphism is given by

$$f_\infty + \varphi_\infty \colon \widetilde{GC}(\mathbb{G}_\infty) \to \widetilde{GC}(\mathbb{G}_0) \oplus \widetilde{GC}(\mathbb{G}_1).$$

We now wish to iterate this quasi-isomorphism to obtain a cube of resolutions that computes the same homology.

Let the crossings of a link L be numbered from 1 to m. Start with a planar projection of L, and convert it into a grid diagram. By applying stabilization and commutation as described in [4; 5; 12], we can require that:

(1) Near every crossing, the diagram is as indicated in Figure 11. For the ith crossing, the associated 6×6 block of cells illustrated is referred to as the ith block.

(2) If $i \neq j$, then the ith block and the jth block occupy disjoint rows and disjoint columns.

Let the resulting grid diagram be $\mathbb{G}$. To each sequence $k_1, k_2, \ldots, k_m$ with $k_i \in \{\infty, 0, 1\}$ for $1 \leq i \leq m$, we associate a grid diagram $\mathbb{G}_{k_1,\ldots,k_m}$. The diagram $\mathbb{G}_{k_1,\ldots,k_m}$ is obtained from $\mathbb{G}$ by replacing the ith block by the appropriate 6×6 block as in
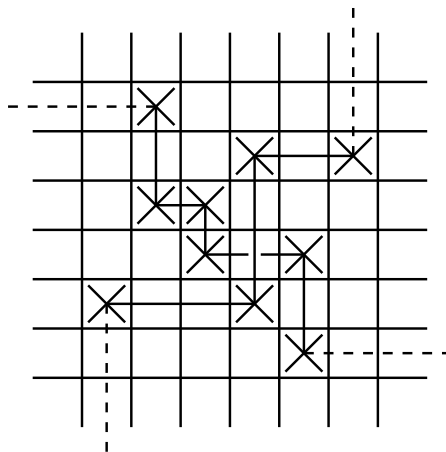

Figure 11: The grid diagram $\mathbb{G}$ of an oriented link L near a crossing. The 6×6 block of cells in the center is the block associated to this crossing.

Figure 2 (where the central 4×4 block is shown), depending on the value of k_i. In particular, $\mathbb{G}_{\infty,\ldots,\infty} = \mathbb{G}$. Let $C_{k_1,\ldots,k_m}$ be the associated chain complex of $\mathbb{G}_{k_1,\ldots,k_m}$, equipped with the differential map. For $1 \leq i \leq m$, we let the edge map

$$f^i_{k_1,\ldots,k_m} \colon C_{k_1,\ldots,k_{i-1},k_i,k_{i+1},\ldots,k_m} \to C_{k_1,\ldots,k_{i-1},k_i+1,k_{i+1},\ldots,k_m}$$

be the map f_k defined in Section 3; this makes sense, since the two chain complexes differ only near a crossing. Analogously, we have the map

$$\varphi^i_{k_1,\ldots,k_m} \colon C_{k_1,\ldots,k_{i-1},k_i,k_{i+1},\ldots,k_m} \to C_{k_1,\ldots,k_{i-1},k_i+2,k_{i+1},\ldots,k_m},$$

which is just the map φ_k defined earlier.

This allows us to define the *big cube of resolutions* of $\mathbb{G}$ to be the complex

$$(\mathrm{BCR}(\mathbb{G}), \partial_{\mathrm{BCR}}) = \left(\bigoplus_{k_i \in \{\infty,0,1\}} C_{k_1,\ldots,k_m}, \right.$$
$$\left. \sum_{k_i \in \{\infty,0,1\}} \left(\partial_{k_1,\ldots,k_m} + \sum_{j\,:\,k_j \in \{\infty,0\}} f^j_{k_1,\ldots,k_m} + \sum_{t\,:\,k_t = \infty} \varphi^t_{k_1,\ldots,k_m} \right) \right),$$

and the *(small) cube of resolutions* of $\mathbb{G}$ to be the complex

$$(\mathrm{CR}(\mathbb{G}), \partial_{\mathrm{CR}}) = \left(\bigoplus_{k_i \in \{0,1\}} C_{k_1,\ldots,k_m}, \sum_{k_i \in \{0,1\}} \left(\partial_{k_1,\ldots,k_m} + \sum_{j\,:\,k_j = 0} f^j_{k_1,\ldots,k_m} \right) \right),$$

which is a subcomplex of $\mathrm{BCR}(\mathbb{G})$. In the cube of resolutions $\mathrm{CR}(\mathbb{G})$, each vertex is associated to a grid diagram in which all crossings have been resolved. The case when there are two crossings is illustrated below:
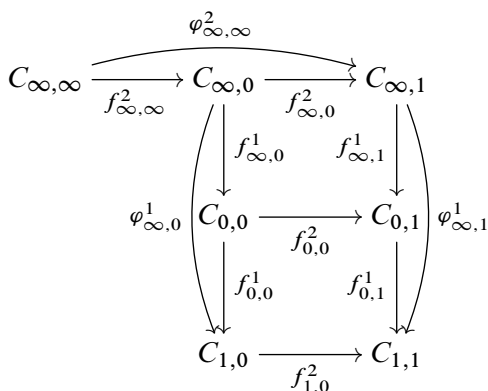
The cube of resolutions $\mathrm{CR}(\mathbb{G})$ consists of the 2×2 square on the lower right. The big cube of resolutions $\mathrm{BCR}(\mathbb{G})$ consists of the whole diagram, together with $C_{0,\infty}$, $C_{1,\infty}$, $f^1_{\infty,\infty}$, $f^1_{0,\infty}$, $f^2_{0,\infty}$, $f^2_{1,\infty}$, $\varphi^1_{\infty,\infty}$, $\varphi^2_{0,\infty}$ and $\varphi^2_{1,\infty}$, which are not shown. (These would all be at the lower left of the diagram.)

Remark 5.1 Neither $\mathrm{BCR}(\mathbb{G})$ nor $\mathrm{CR}(\mathbb{G})$ contains diagonal maps, eg a map that goes from $C_{\infty,0}$ to $C_{0,1}$ or $C_{1,1}$. This is in stark contrast with cubes of resolutions in many other contexts. For example, in [17], where the technique of spectral sequences was first applied to Heegaard Floer homology, there are diagonal maps in both the big $\{\infty, 0, 1\}^m$ cube and the small $\{0, 1\}^m$ cube. Such diagonal maps are needed because the edge maps f and φ only commute *up to chain homotopy*. Below, Lemma 5.3 will guarantee that our edge maps commute *on the nose*, allowing us to define the diagonal maps to be zero.

In the case with two crossings, observe that $C_{\infty,\infty}$ is quasi-isomorphic to the mapping cone of $f^2_{\infty,0}$ via $f^2_{\infty,\infty} + \varphi^2_{\infty,\infty}$. The fact that the diagram commutes now immediately implies that

(1) the cube of resolutions $\mathrm{CR}(\mathbb{G})$ is a chain complex;

(2) the sum $f^1_{\infty,0} + f^1_{\infty,1} + \varphi^1_{\infty,0} + \varphi^1_{\infty,1}$ is a chain map from the mapping cone of $f^2_{\infty,0}$ to the cube of resolutions $\mathrm{CR}(\mathbb{G})$; and

(3) this chain map is a quasi-isomorphism.

(To see the last statement, observe that if $f\colon C_1 \to C_2$ and $f'\colon C'_1 \to C'_2$ are quasi-isomorphisms, and if there exist maps $g_1\colon C_1 \to C'_1$ and $g_2\colon C_2 \to C'_2$ such that the diagram

$$
\begin{array}{ccc}
C_1 & \xrightarrow{\ f\ } & C_2 \\
{\scriptstyle g_1}\downarrow & & \downarrow{\scriptstyle g_2} \\
C'_1 & \xrightarrow{\ f'\ } & C'_2
\end{array}
$$

commutes, then $f + f'$ is a quasi-isomorphism between the mapping cone of g_1 and that of g_2.) Thus, we see that $C_{\infty,\infty}$ is quasi-isomorphic to $\mathrm{CR}(\mathbb{G})$.

The general case is similar; to be precise, our claim is the following.

Proposition 5.2 *The cubes of resolutions* $\mathrm{BCR}(\mathbb{G}; \mathbb{F}_2)$ *and* $\mathrm{CR}(\mathbb{G}; \mathbb{F}_2)$ *are indeed chain complexes. Moreover,* $\mathrm{CR}(\mathbb{G}; \mathbb{F}_2)$ *is quasi-isomorphic to* $\widetilde{\mathrm{GC}}(\mathbb{G}; \mathbb{F}_2)$. *As a consequence,* $\mathrm{BCR}(\mathbb{G}; \mathbb{F}_2)$ *is acyclic.*

As mentioned, the main ingredient in proving Proposition 5.2 is the following lemma.

Lemma 5.3 *All maps involved commute. Precisely,*

$$
f^{i_2}_{k_1,\dots,k_{i_1}+1,\dots,k_m} \circ f^{i_1}_{k_1,\dots,k_{i_1},\dots,k_m} = f^{i_1}_{k_1,\dots,k_{i_2}+1,\dots,k_m} \circ f^{i_2}_{k_1,\dots,k_{i_2},\dots,k_m},
$$

$$
\varphi^{i_2}_{k_1,\dots,k_{i_1}+1,\dots,k_m} \circ f^{i_1}_{k_1,\dots,k_{i_1},\dots,k_m} = f^{i_1}_{k_1,\dots,k_{i_2}+2,\dots,k_m} \circ \varphi^{i_2}_{k_1,\dots,k_{i_2},\dots,k_m}.
$$

Proof Inspecting the 6×6 block in Figure 11, we see that there is an X near each corner of the block, and so each allowed polygon defined in Section 3 counted in a chain map or a chain homotopy can only leave the block either horizontally or vertically. If it leaves the block horizontally, then it is contained in the rows that the block spans; if it leaves the block vertically, then it is contained in the columns that the block spans. This shows that if two polygons from two different crossings share a corner, one must be long and horizontal, and the other long and vertical; in such cases, the composite domain always has an obvious alternative decomposition. The cases where the two polygons are disjoint or have overlapping interiors are obvious. □

Proof of Proposition 5.2 Exactly as in the case with two crossings, Lemma 5.3 implies that the cube of resolutions is indeed a chain complex, and that all appropriate maps are chain maps. We proceed by induction: at each step, we claim that the chain complexes

$$\left(\bigoplus_{k_i \in \{0,1\}} C_{\infty,\dots,\infty,k_{t+1},\dots,k_m}, \sum_{k_i \in \{0,1\}} \left(\partial_{\infty,\dots,\infty,k_{t+1},\dots,k_m} + \sum_{j:k_j=0} f^j_{\infty,\dots,\infty,k_{t+1},\dots,k_m} \right) \right)$$

and

$$\left(\bigoplus_{k_i \in \{0,1\}} C_{\infty,\dots,\infty,k_t,\dots,k_m}, \sum_{k_i \in \{0,1\}} \left(\partial_{\infty,\dots,\infty,k_t,\dots,k_m} + \sum_{j:k_j=0} f^j_{\infty,\dots,\infty,k_t,\dots,k_m} \right) \right)$$

are quasi-isomorphic. The quasi-isomorphism is given by

$$\sum_{k_i \in \{0,1\}} f^t_{\infty,\dots,\infty,k_{t+1},\dots,k_m} + \sum_{k_i \in \{0,1\}} \varphi^t_{\infty,\dots,\infty,k_{t+1},\dots,k_m}.$$

This map is a quasi-isomorphism by the induction hypothesis and by the comment after (3) in the case with two crossings above. □

Corollary 1.4 follows from Proposition 5.2.

Remark 5.4 Over $\mathbb{Z}$, for the cube of resolutions to be a chain complex, the analogue of Lemma 5.3 over $\mathbb{Z}$ should presumably state that the maps involved *anticommute*. However, if we denote by ρ^i (resp. τ^i) the maps defined by the rectangle-like (resp. triangle-like) polygons associated to the ith crossing following the definitions in Section 4, then we have:

(1) $\rho^2 \circ \rho^1 = -\rho^1 \circ \rho^2$

(2) $\rho^2 \circ \tau^1 = -\tau^1 \circ \rho^2$

(3) $\tau^2 \circ \rho^1 = -\rho^1 \circ \tau^2$

(4) $\tau^2 \circ \tau^1 = \tau^1 \circ \tau^2$

Since *only* the maps defined by triangle-like polygons commute, the author has thus far been unable to prove a version of Lemma 5.3, and therefore Proposition 5.2, over $\mathbb{Z}$.

6 Quasialternating links

We now describe an application of the skein exact triangle. To begin, we must first define the δ–grading on knot Floer homology. The δ–grading is closely related to the Maslov and Alexander gradings; in view of that, in this section we revert to the traditional notation with both Os and Xs, and denote the set of Os by $\mathbb{O}$ and that of Xs by $\mathbb{X}$.

The following formulation is found in [12]. Given two collections A and B of finitely many points in the plane, let

$$\mathcal{J}(A, B) = \tfrac{1}{2}\#\{((a_1, a_2), (b_1, b_2)) \in A \times B \mid a_1 < b_1 \text{ and } a_2 < b_2\}$$
$$+ \tfrac{1}{2}\#\{((a_1, a_2), (b_1, b_2)) \in A \times B \mid b_1 < a_1 \text{ and } b_2 < a_2\}.$$

Treating $\boldsymbol{x} \in \boldsymbol{S}(\mathbb{G})$ as a collection of points with integer coordinates in a fundamental domain for $\mathbb{T}$, and similarly $\mathbb{O}$ and $\mathbb{X}$ as collections of points in the plane with half-integer coordinates, the Maslov grading of a generator is given by

$$M(\boldsymbol{x}) = \mathcal{J}(\boldsymbol{x}, \boldsymbol{x}) - 2\mathcal{J}(\boldsymbol{x}, \mathbb{O}) + \mathcal{J}(\mathbb{O}, \mathbb{O}) + 1,$$

while the Alexander grading is given by

$$A(\boldsymbol{x}) = \mathcal{J}(\boldsymbol{x}, \mathbb{X}) - \mathcal{J}(\boldsymbol{x}, \mathbb{O}) - \tfrac{1}{2}\mathcal{J}(\mathbb{X}, \mathbb{X}) + \tfrac{1}{2}\mathcal{J}(\mathbb{O}, \mathbb{O}) - \tfrac{1}{2}(n - 1),$$

where n is the size of the grid diagram. Now the δ–grading is just

$$\delta(\boldsymbol{x}) = A(\boldsymbol{x}) - M(\boldsymbol{x});$$

in other words, we have

$$\delta(\boldsymbol{x}) = -\mathcal{J}(\boldsymbol{x}, \boldsymbol{x}) + \mathcal{J}(\boldsymbol{x}, \mathbb{X}) + \mathcal{J}(\boldsymbol{x}, \mathbb{O}) - \tfrac{1}{2}\mathcal{J}(\mathbb{X}, \mathbb{X}) - \tfrac{1}{2}\mathcal{J}(\mathbb{O}, \mathbb{O}) - \tfrac{1}{2}(n + 1).$$

These gradings do not depend on the choice of the fundamental domain; moreover, they agree with the original definitions in terms of pseudoholomorphic representatives.

It has been observed that, for many classes of links, the knot Floer homology over $R = \mathbb{F}_2$ or $\mathbb{Z}$ is a free R–module supported in only one δ–grading, which motivates the following definition by Rasmussen [19; 20] and Manolescu and Ozsváth [10]:

Definition 6.1 Let $R = \mathbb{F}_2$ or $\mathbb{Z}$. A link L is *Floer homologically thin* over R if $\widehat{\mathrm{HFK}}(L; R)$ is a free R–module supported in only one δ–grading. If in addition the δ–grading equals $-\tfrac{1}{2}\sigma(L)$, where $\sigma(L)$ is the signature of the link, then we say that L is *Floer homologically σ–thin*.

Manolescu and Ozsváth [10] showed that a class of links which is a natural generalization of alternating knots has the homologically σ–thin property over $\mathbb{F}_2$. Precisely, we recall the following definition from [17]:

Definition 6.2 The set of *quasialternating links* $\mathcal{Q}$ is the smallest set of links satisfying the following properties:

(1) The unknot is in $\mathcal{Q}$.

(2) If L_∞ is a link that admits a projection with a crossing such that
   (a) both resolutions L_0 and L_1 at that crossing are in $\mathcal{Q}$, and
   (b) $\det(L_\infty) = \det(L_0) + \det(L_1)$,
   then L_∞ is in $\mathcal{Q}$.

The result of Manolescu and Ozsváth [10] is then the following statement.

Theorem 6.3 (Manolescu and Ozsváth) *Quasialternating links are Floer homologically σ–thin over $\mathbb{F}_2$.*

The proof of the theorem is essentially an application of Manolescu's unoriented skein exact triangle; the main work is in tracking the changes in the δ–grading of the maps involved. The same idea works in the current context as well: with grid diagrams, we may similarly track the changes in the δ–grading, defined by the formula above. Of course, in our case, we will be proving the result for $\widehat{\mathrm{GH}}$ of a link instead of $\widehat{\mathrm{HFK}}$, as in Theorem 1.5. From this, we will obtain Theorem 1.6, a strengthened version of Theorem 6.3.

To begin, fix a crossing c_0 in the planar diagram of a link L_∞. Let L_+ be the link with a positive crossing at c_0, and L_- the link with a negative crossing; then either $L_\infty = L_+$ or $L_\infty = L_-$. Let L_h and L_v be the unoriented and oriented resolutions of L_∞ at c_0 respectively, and choose an arbitrary orientation for L_h. This is illustrated in Figure 12. Comparing with Figure 1, if $L_\infty = L_+$, then $L_0 = L_h$ and $L_1 = L_v$; if instead $L_\infty = L_-$, then $L_0 = L_v$ and $L_1 = L_h$.

Denote by D_+, D_-, D_v, D_h the planar diagrams of L_+, L_-, L_v, L_h, differing from each other only at c_0. The following lemma is used in [10]; for L_+, the first equality is
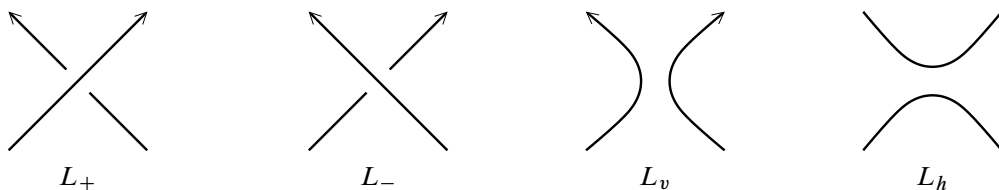

Figure 12: L_+, L_-, L_h and L_v near a point

proven by Murasugi [13], while the second is also inspired by a result of Murasugi [14]. The equalities for L_- are similarly obtained.

Lemma 6.4 *Suppose that* $\det(L_v), \det(L_h) > 0$. *Let e denote the difference between the number of negative crossings in D_h and the number of such crossings in D_+. If* $\det(L_+) = \det(L_v) + \det(L_h)$, *then*

   (1) $\sigma(L_v) - \sigma(L_+) = 1$,

   (2) $\sigma(L_h) - \sigma(L_+) = e$.

If $\det(L_-) = \det(L_v) + \det(L_h)$, *then*

   (1) $\sigma(L_v) - \sigma(L_-) = -1$,

   (2) $\sigma(L_h) - \sigma(L_-) = e$.

Now we investigate the changes in the δ–grading in the maps f_k defined in Section 3 and Section 4.

Given two grid diagrams $\mathbb{G}, \mathbb{G}'$ of the same size n, we can think of them as being on the same grid (ie consisting of the same horizontal and vertical circles) but having different Os and Xs; therefore, we can write $\mathbb{G} = (n, \mathbb{O}, \mathbb{X})$ and $\mathbb{G}' = (n, \mathbb{O}', \mathbb{X}')$. This allows us to identify $S(\mathbb{G})$ and $S(\mathbb{G}')$, by viewing each generator $x \in S(\mathbb{G})$ as the permutation σ_x referred to in Remark 4.3. In this point of view, we will write $\delta_{\mathbb{G}}(x)$ and $\delta_{\mathbb{G}'}(x)$ to denote the gradings defined by applying the δ–grading formula to $(\mathbb{O}, \mathbb{X})$ and $(\mathbb{O}', \mathbb{X}')$, respectively.

In particular, for the rest of this section, we will view $\mathbb{G}_\infty, \mathbb{G}_0, \mathbb{G}_1$ in this manner.

Lemma 6.5 *Let $x \in S(\mathbb{G})$ be a fixed generator in a grid diagram $\mathbb{G} = (n, \mathbb{O}, \mathbb{X})$. Then:*

   (1) *If there is an empty rectangle r from x to y, possibly containing Os and Xs, then $\delta_{\mathbb{G}}(y) = \delta_{\mathbb{G}}(x) + 1 - \#(\text{Int}(r) \cap (\mathbb{O} \cup \mathbb{X}))$.*

   (2) *Suppose $\mathbb{G}' = (n, \mathbb{O}', \mathbb{X})$ is a grid diagram identical to $\mathbb{G}$ except in two adjacent columns, where the horizontal positions of a pair of O markers are interchanged, as in Figure 13. Then*

   (a) $\delta_{\mathbb{G}'}(x) - \delta_{\mathbb{G}}(x) = -\frac{1}{2}$ *if, in $\mathbb{G}$, the component of x on the vertical circle between the markers lies to the northeast of one marker and to the southwest of the other (the component of x indicated in the diagrams by a solid point);*

   (b) $\delta_{\mathbb{G}'}(x) - \delta_{\mathbb{G}}(x) = \frac{1}{2}$ *otherwise (the component of x indicated by a hollow point).*

   The same statement holds if, instead, the horizontal positions of a pair of X markers are interchanged, with $\mathbb{G}' = (n, \mathbb{O}, \mathbb{X}')$.

(3) *If the diagram $\mathbb{G}'$ is obtained from $\mathbb{G}$ by reversing the orientation of a component K of L, then $\delta_{\mathbb{G}'}(\boldsymbol{x}) - \delta_{\mathbb{G}}(\boldsymbol{x}) = -\frac{\epsilon}{2}$, where ϵ is the difference between the number of negative crossings in $\mathbb{G}'$ and the number of such crossings in $\mathbb{G}$.*
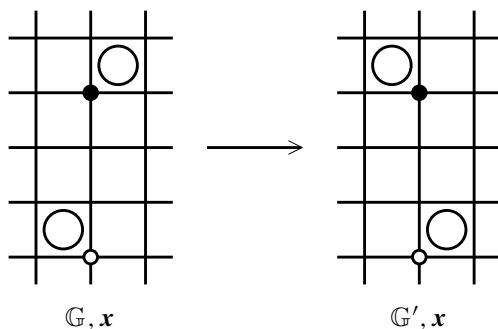

Figure 13: Moving two markers across a vertical circle. Observe that before the move, the solid point lies to the northeast of one of the Os and to the southwest of the other, thus forming two southwest–northeast pairs with the markers that are destroyed in the move. The hollow point forms the same number of pairs with the markers before and after the move.

Proof Recall that

$$\delta(\boldsymbol{x}) = -\mathcal{J}(\boldsymbol{x}, \boldsymbol{x}) + \mathcal{J}(\boldsymbol{x}, \mathbb{X}) + \mathcal{J}(\boldsymbol{x}, \mathbb{O}) - \tfrac{1}{2}\mathcal{J}(\mathbb{X}, \mathbb{X}) - \tfrac{1}{2}\mathcal{J}(\mathbb{O}, \mathbb{O}) - \tfrac{1}{2}(n+1).$$

Observe that $\mathcal{J}(A, B)$ is the number of southwest–northeast pairs between A and B, divided by two. We make the following observations.

(1) Observe that the last three terms in $\delta(\boldsymbol{x})$ and $\delta(\boldsymbol{y})$ are identical. Switching from $\boldsymbol{x}$ to $\boldsymbol{y}$ destroys exactly one southwest–northeast pair, which is counted twice and contributes $+1$ to $\mathcal{J}(\boldsymbol{x}, \boldsymbol{x})$. For every O or X inside $\mathrm{Int}(r)$, switching from $\boldsymbol{x}$ to $\boldsymbol{y}$ destroys two southwest–northeast pairs, each counted once, that contribute $+1$ to $\mathcal{J}(\boldsymbol{x}, \mathbb{X}) + \mathcal{J}(\boldsymbol{x}, \mathbb{O})$.

(2) Consider the first case, where $\mathbb{G} = (n, \mathbb{O}, \mathbb{X})$ and $\mathbb{G}' = (n, \mathbb{O}', \mathbb{X})$, as in Figure 13. We first see that $\mathcal{J}(\mathbb{O}', \mathbb{O}') - \mathcal{J}(\mathbb{O}, \mathbb{O}) = -1$. If the component of $\boldsymbol{x}$ on the vertical circle lies to the northeast of one marker and to the southwest of the other, then $\mathcal{J}(\boldsymbol{x}, \mathbb{O}') - \mathcal{J}(\boldsymbol{x}, \mathbb{O}) = -1$; otherwise, this quantity is 0. All other terms in $\delta_{\mathbb{G}}(\boldsymbol{x})$ and $\delta_{\mathbb{G}'}(\boldsymbol{x})$ are identical. The second case is entirely analogous.

(3) This is simply a restatement of [12, Proposition 5.4].

This completes the proof of the lemma.   □

The following is an easy consequence of Lemma 6.5(1)–(2).

Lemma 6.6 *Suppose $\mathbb{G}_k$ and $\mathbb{G}_{k+1}$ are grid presentations of two links with compatible orientations (so $\mathbb{G}_k$ and $\mathbb{G}_{k+1}$ have compatible sets of Os), and $f_k\colon \mathbb{G}_k \to \mathbb{G}_{k+1}$ is the map defined in Sections 3 and 4. If $x \in S(\mathbb{G}_k)$, and $y \in S(\mathbb{G}_{k+1})$ appears in $f_k(x)$, then $\delta_{\mathbb{G}_{k+1}}(y) - \delta_{\mathbb{G}_k}(x) = +\frac{1}{2}$.*

Proof Note first that the grid diagrams $\mathbb{G}_k = (n, \mathbb{O}, \mathbb{X})$ and $\mathbb{G}_{k+1} = (n, \mathbb{O}', \mathbb{X}')$ are related as in Lemma 6.5(2). Refer to Figure 14. Without loss of generality, assume that the two relevant markers are Os. (The case where they are Xs is completely analogous.) Label the two markers in $\mathbb{O}$ by O_1 and O_2, so that O_1 lies to the northeast of O_2; similarly, label the markers in $\mathbb{O}'$ by O_1' and O_2', so that O_1' lies to the northwest of O_2'. In the current framework, β_∞, β_0 and β_1 are all represented by the vertical circle β in the middle. Let x be the β–component of x.

Suppose $y \in S(\mathbb{G}_{k+1})$ appears in $f_k(x)$. Then

$$\delta_{\mathbb{G}_{k+1}}(y) - \delta_{\mathbb{G}_k}(x) = (\delta_{\mathbb{G}_{k+1}}(x) - \delta_{\mathbb{G}_k}(x)) + (\delta_{\mathbb{G}_{k+1}}(y) - \delta_{\mathbb{G}_{k+1}}(x)).$$

There are two cases, as follows.

Suppose there is an empty pentagon p from x to y; in the framework described in this section, it can in fact be viewed as an empty rectangle r from x to y in $\mathbb{G}_{k+1}$. Observe that the horizontal circles divide $\mathbb{T}$ into a number of components; let A be the unique component containing both O_1 in $\mathbb{G}_k$ and O_1' in $\mathbb{G}_{k+1}$. Since the boundary of p contains u_k (cf Figure 3), which lies in A, the boundary of r must contain $\beta \cap A$. Therefore, one of two scenarios must be true:

(1) The point x lies to the northeast of O_2 and to the southwest of O_1. Then $\mathrm{Int}(r) \cap (\mathbb{O} \cup \mathbb{X}) = \varnothing$. By Lemma 6.5(2)(a), $\delta_{\mathbb{G}_{k+1}}(x) - \delta_{\mathbb{G}_k}(x) = -\frac{1}{2}$, and by Lemma 6.5(1), $\delta_{\mathbb{G}_{k+1}}(y) - \delta_{\mathbb{G}_{k+1}}(x) = 1$. This is illustrated by the top row of Figure 14.

(2) The point x lies elsewhere. Then $\mathrm{Int}(r) \cap (\mathbb{O} \cup \mathbb{X})$ is either $\{O_1'\}$ or $\{O_2'\}$. By Lemma 6.5(2)(b), $\delta_{\mathbb{G}_{k+1}}(x) - \delta_{\mathbb{G}_k}(x) = +\frac{1}{2}$, and by Lemma 6.5(1), we have $\delta_{\mathbb{G}_{k+1}}(y) - \delta_{\mathbb{G}_{k+1}}(x) = 1 - 1 = 0$. This is illustrated by the middle row of Figure 14.

Either way, we get that $\delta_{\mathbb{G}_{k+1}}(y) - \delta_{\mathbb{G}_k}(x) = +\frac{1}{2}$.

Suppose there is a triangle p from x to y; then, in the framework of this section, $x = y$, and so $\delta_{\mathbb{G}_{k+1}}(y) - \delta_{\mathbb{G}_{k+1}}(x) = 0$. Since the boundary of p contains v_k (cf Figure 3), we see that $\mathrm{Int}(p) \subset \mathrm{Int}(t_k) \cup \mathrm{Int}(t_{k+1})$. This implies that x cannot lie both to the northeast of O_2 and to the southwest of O_1. Thus, by Lemma 6.5(2)(b), $\delta_{\mathbb{G}_{k+1}}(x) - \delta_{\mathbb{G}_k}(x) = +\frac{1}{2}$. This case is illustrated by the bottom row of Figure 14. $\square$

We can now prove a graded version of Theorem 1.3.

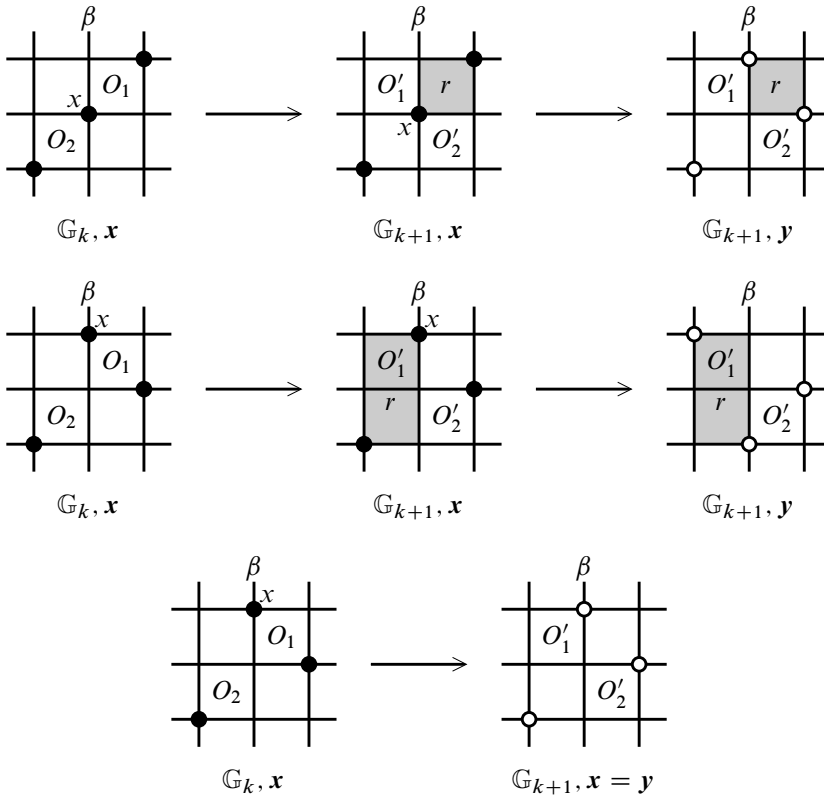Figure 14: Computing the δ–grading change under f_k when $\mathbb{G}_k$ and $\mathbb{G}_{k+1}$ have compatible orientations. The top and middle rows show the case when the polygon p being counted is a pentagon, while the bottom row shows the case when p is a triangle. In both cases, $\boldsymbol{y}$ appears in $f_k(\boldsymbol{x})$. Note that there may be multiple horizontal circles between the Os, which are omitted for the sake of simplicity, in each of the figures above.

Proposition 6.7 *With respect to the δ–grading the skein exact sequence in Theorem 1.3 can be written as*

$$\cdots \to \widehat{GH}_{*-\frac{1}{2}}(L_v; R) \otimes V^{n-\ell_v} \to \widehat{GH}_*(L_+; R) \otimes V^{n-\ell_+}$$
$$\to \widehat{GH}_{*-\frac{e}{2}}(L_h; R) \otimes V^{n-\ell_h} \to \widehat{GH}_{*-\frac{1}{2}+1}(L_v; R) \otimes V^{n-\ell_v} \to \cdots$$

and

$$\cdots \to \widehat{GH}_{*-\frac{e}{2}}(L_h; R) \otimes V^{n-\ell_h} \to \widehat{GH}_*(L_-; R) \otimes V^{n-\ell_-}$$
$$\to \widehat{GH}_{*+\frac{1}{2}}(L_v; R) \otimes V^{n-\ell_v} \to \widehat{GH}_{*-\frac{e}{2}+1}(L_h; R) \otimes V^{n-\ell_h} \to \cdots ,$$

where $R = \mathbb{F}_2$ or $\mathbb{Z}$, V is a free module of rank 2 over R with grading zero, and e is as in the statement of Lemma 6.4.

Proof Suppose L_∞ has a positive crossing at c_0, so that $L_+ = L_\infty$, $L_v = L_1$ and $L_h = L_0$. Let $\mathbb{G}_\infty, \mathbb{G}_0, \mathbb{G}_1$ be grid diagrams for L_∞, L_0, L_1 respectively, differing with each other only at c_0 as in Figure 2. Note that in Figure 2 only Xs are used as markers, whereas in the present context both Xs and Os are used. Then we are to prove that in the exact sequence

$$\cdots \to \widetilde{GH}(\mathbb{G}_1) \xrightarrow{(f_1)_*} \widetilde{GH}(\mathbb{G}_\infty) \xrightarrow{(f_\infty)_*} \widetilde{GH}(\mathbb{G}_0) \xrightarrow{(f_0)_*} \widetilde{GH}(\mathbb{G}_1) \to \cdots,$$

the map f_1 shifts the δ–grading by $+\frac{1}{2}$, f_∞ by $-\frac{\epsilon}{2}$, and f_0 by $+\frac{1}{2}(e+1)$.

Refer to Figure 15. Since L_1 and L_∞ have compatible orientations, Lemma 6.6 shows that the map f_1 shifts the δ–grading by $+\frac{1}{2}$.
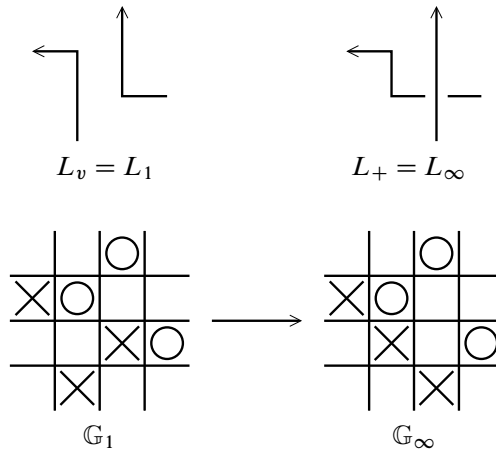

Figure 15: A straightforward application of Lemma 6.6 gives the δ–grading shift of f_1

Let us now focus on f_∞. Let $\boldsymbol{x} \in \boldsymbol{S}(\mathbb{G}_\infty)$ be a generator, and suppose $\boldsymbol{y} \in \boldsymbol{S}(\mathbb{G}_0)$ appears in $f_\infty(\boldsymbol{x})$. We proceed according to whether the two strands of the link L_+ meeting at the crossing c_0 belong to different components, or to the same component, of L_+, as follows.

Suppose the strands belong to different components; see Figure 16. Starting from $\mathbb{G}_\infty$, we can reverse the orientation of one of the two components to obtain a new diagram $\mathbb{G}'_\infty$; then we can write

$$\delta_{\mathbb{G}_0}(\boldsymbol{y}) - \delta_{\mathbb{G}_\infty}(\boldsymbol{x}) = (\delta_{\mathbb{G}'_\infty}(\boldsymbol{x}) - \delta_{\mathbb{G}_\infty}(\boldsymbol{x})) + (\delta_{\mathbb{G}_0}(\boldsymbol{y}) - \delta_{\mathbb{G}'_\infty}(\boldsymbol{x})).$$

By Lemma 6.5(3), we have $\delta_{\mathbb{G}'_\infty}(\boldsymbol{x}) - \delta_{\mathbb{G}_\infty}(\boldsymbol{x}) = -\frac{\epsilon}{2}$, where ϵ is the difference between the number of negative crossings in $\mathbb{G}'_\infty$ and the number of such crossings in $\mathbb{G}_\infty$ (which represents L_+). Now observe that $\mathbb{G}'_\infty$ and $\mathbb{G}_0$ have compatible orientations;
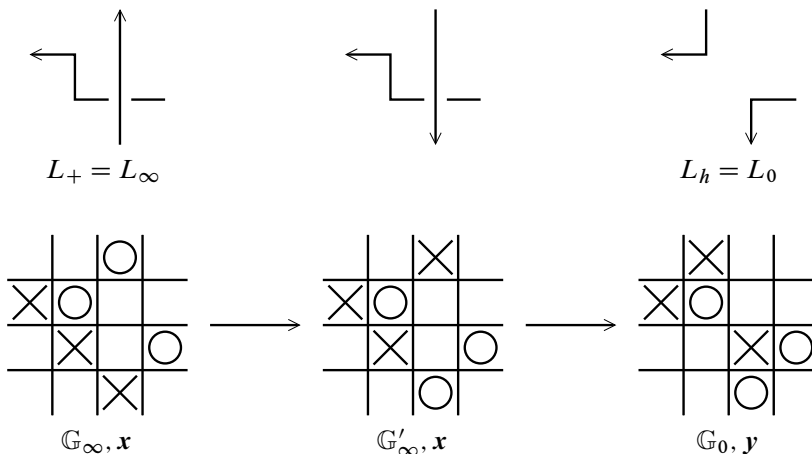
Figure 16: Computation of the δ–grading shift of f_∞, when the two strands meeting at c_0 belong to different components. The generators x and y are not shown, as their positions do not affect the argument.

also, $\mathbb{G}'_\infty$ has one more negative crossing, near c_0, than does $\mathbb{G}_0$ (which represents L_h). Therefore, $\epsilon = e + 1$. Furthermore, the fact that $\mathbb{G}'_\infty$ and $\mathbb{G}_0$ have compatible orientations implies that Lemma 6.6 can be applied, so $\delta_{\mathbb{G}_0}(y) - \delta_{\mathbb{G}'_\infty}(x) = +\frac{1}{2}$. Thus,

$$\delta_{\mathbb{G}_0}(y) - \delta_{\mathbb{G}_\infty}(x) = -\tfrac{1}{2}(e+1) + \tfrac{1}{2} = -\tfrac{e}{2}.$$

Suppose now the strands belong to the same component. As in the proof of Lemma 6.6, we write

$$\delta_{\mathbb{G}_0}(y) - \delta_{\mathbb{G}_\infty}(x) = (\delta_{\mathbb{G}_0}(x) - \delta_{\mathbb{G}_\infty}(x)) + (\delta_{\mathbb{G}_0}(y) - \delta_{\mathbb{G}_0}(x)).$$

Note that this is different from the equation we use when the strands belong to different components. We first compute $\delta_{\mathbb{G}_0}(x) - \delta_{\mathbb{G}_\infty}(x)$; see Figure 17. Since the two strands in L_+ belong to the same component, the two strands in L_v must belong to different components. Therefore, we can reverse the orientation of one of these components in $\mathbb{G}_1$ (which represents L_v) to obtain a new diagram $\mathbb{G}'_1$; then

$$\delta_{\mathbb{G}_0}(x) - \delta_{\mathbb{G}_\infty}(x) = (\delta_{\mathbb{G}_1}(x) - \delta_{\mathbb{G}_\infty}(x)) + (\delta_{\mathbb{G}'_1}(x) - \delta_{\mathbb{G}_1}(x)) + (\delta_{\mathbb{G}_0}(x) - \delta_{\mathbb{G}'_1}(x)).$$

Let x be the β–component of x. We can now compute, by Lemma 6.5(2),

$$\delta_{\mathbb{G}_1}(x) - \delta_{\mathbb{G}_\infty}(x) = \begin{cases} +\frac{1}{2} & \text{if } x \text{ lies at the hollow square in Figure 17,} \\ -\frac{1}{2} & \text{otherwise.} \end{cases}$$

Now by Lemma 6.5(3), $\delta_{\mathbb{G}'_1}(x) - \delta_{\mathbb{G}_1}(x) = -\frac{\epsilon}{2}$, where ϵ is the difference between the number of negative crossings in $\mathbb{G}'_1$ and the number of such crossings in $\mathbb{G}_1$. Observe

that $\mathbb{G}_1$ and $\mathbb{G}_\infty$ (which represents L_+) have compatible orientations and hence the same number of negative crossings. Similarly, $\mathbb{G}'_1$ and $\mathbb{G}_0$ have compatible orientations and hence the same number of negative crossings. Therefore, we see that $\epsilon = e$. Next, again by Lemma 6.5(2), we have

$$\delta_{\mathbb{G}_0}(\boldsymbol{x}) - \delta_{\mathbb{G}'_1}(\boldsymbol{x}) = \begin{cases} -\frac{1}{2} & \text{if } x \text{ lies at the solid point, hollow point} \\ & \text{or hollow square in Figure 17;} \\ +\frac{1}{2} & \text{otherwise.} \end{cases}$$

Combining these calculations, we conclude that

$$\delta_{\mathbb{G}_0}(\boldsymbol{x}) - \delta_{\mathbb{G}_\infty}(\boldsymbol{x}) = \begin{cases} -\frac{1}{2}(e+2) & \text{if } x \text{ lies at the solid point or hollow point} \\ & \text{in Figure 17;} \\ -\frac{e}{2} & \text{otherwise.} \end{cases}$$

We now return to computing $\delta_{\mathbb{G}_0}(\boldsymbol{y}) - \delta_{\mathbb{G}_\infty}(\boldsymbol{x})$.

Suppose there is an empty pentagon p from $\boldsymbol{x}$ to $\boldsymbol{y}$; in the framework described in this section, it can in fact be viewed as an empty rectangle r from $\boldsymbol{x}$ to $\boldsymbol{y}$ in $\mathbb{G}_0$. By an argument similar to that in the proof of Lemma 6.6, one of two scenarios must hold:

(1) If the point x lies at the solid point or at the hollow point in Figure 17, then $\text{Int}(r) \cap (\mathbb{O} \cup \mathbb{X}) = \varnothing$. By Lemma 6.5(1), $\delta_{\mathbb{G}_0}(\boldsymbol{y}) - \delta_{\mathbb{G}_0}(\boldsymbol{x}) = 1$.

(2) If the point x lies elsewhere, then $\text{Int}(r) \cap (\mathbb{O} \cup \mathbb{X})$ contains exactly one point. By Lemma 6.5(1), $\delta_{\mathbb{G}_0}(\boldsymbol{y}) - \delta_{\mathbb{G}_0}(\boldsymbol{x}) = 1 - 1 = 0$.

Combining with our earlier calculation, we get that $\delta_{\mathbb{G}_0}(\boldsymbol{y}) - \delta_{\mathbb{G}_\infty}(\boldsymbol{x}) = -\frac{e}{2}$.

Suppose there is a triangle p from $\boldsymbol{x}$ to $\boldsymbol{y}$; then, in the framework of this section, $\boldsymbol{x} = \boldsymbol{y}$, and so $\delta_{\mathbb{G}_0}(\boldsymbol{y}) - \delta_{\mathbb{G}_0}(\boldsymbol{x}) = 0$. Since the boundary of p contains v_∞ (cf Figure 3), we see that $\text{Int}(p) \subset \text{Int}(t_\infty) \cup \text{Int}(t_0)$. This implies that x cannot lie at the solid point or at the hollow point in Figure 17. Therefore, by our earlier calculation, again we have $\delta_{\mathbb{G}_0}(\boldsymbol{y}) - \delta_{\mathbb{G}_\infty}(\boldsymbol{x}) = -\frac{e}{2}$.

Finally, a calculation analogous to that for f_∞ can be done for f_0, and we obtain, in this case, that the shift in the δ–grading is $+\frac{1}{2}(e+1)$.

The case when $L_\infty = L_-$ has a negative crossing at c_0 is similar. $\qquad\square$

Remark 6.8 The proof above only shows that the maps f_k are graded chain maps in the exact sequence. To show that $\widetilde{\text{GC}}(\mathbb{G}_k)$ is *graded* quasi-isomorphic to the mapping cone of f_{k+1} (cf Section 5), we would have to show analogous statements for the chain homotopies φ_k also. The proof of such statements are omitted here, but are completely analogous to the proof of Proposition 6.7.
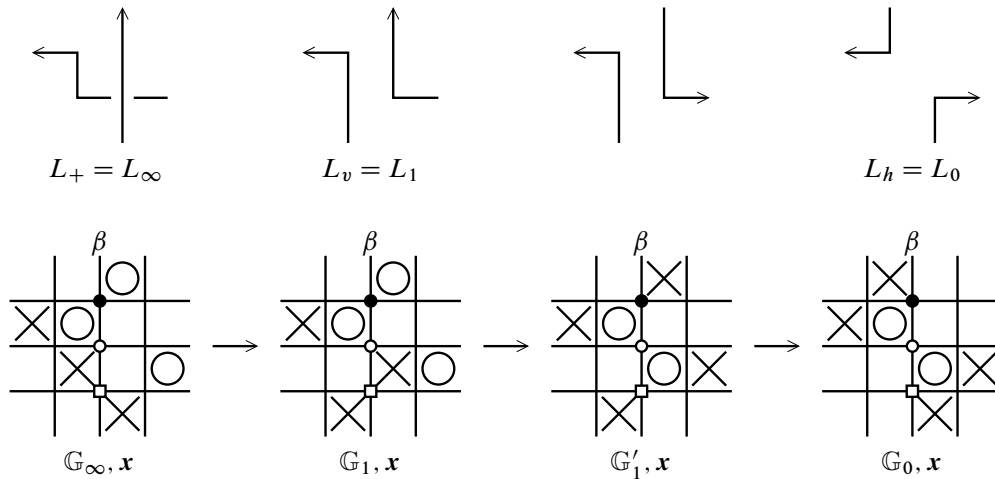
Figure 17: Computation of the δ–grading shift of f_∞, when the two strands meeting at c_0 belong to the same component. The computation depends on the position of x, the β–component of $\boldsymbol{x}$; the special cases are indicated by the solid point, the hollow point, and the hollow square.

Proof of Theorem 1.5 This is just a restatement of Proposition 6.7, taking into account the result of Lemma 6.4.   □

Proof of Theorem 1.6 By definition, every quasialternating link has nonzero determinant. It can easily be checked that the unknot is homologically σ–thin. If L_0 and L_1 are resolutions of L_∞ that are quasialternating, then by induction, L_0 and L_1 are homologically σ–thin. The exact sequence in Theorem 1.5 collapses into short exact sequences, all but one of which are zero. Thus L_∞ is also homologically σ–thin.   □

References

[1]   **J A Baldwin**, *On the spectral sequence from Khovanov homology to Heegaard Floer homology*, Int. Math. Res. Not. 2011 (2011) 3426–3470 MR

[2]   **J A Baldwin**, **A S Levine**, *A combinatorial spanning tree model for knot Floer homology*, Adv. Math. 231 (2012) 1886–1939 MR

[3]   **D Bar-Natan**, *On Khovanov's categorification of the Jones polynomial*, Algebr. Geom. Topol. 2 (2002) 337–370 MR

[4]   **P R Cromwell**, *Embedding knots and links in an open book, I: Basic properties*, Topology Appl. 64 (1995) 37–58 MR

[5]   **I A Dynnikov**, *Arc-presentations of links: monotonic simplification*, Fund. Math. 190 (2006) 29–76 MR

[6] **M Khovanov**, *A categorification of the Jones polynomial*, Duke Math. J. 101 (2000) 359–426 MR

[7] **M Khovanov**, *A functor-valued invariant of tangles*, Algebr. Geom. Topol. 2 (2002) 665–741 MR

[8] **R Lipshitz**, **P S Ozsváth**, **D P Thurston**, *Bordered Floer homology and the spectral sequence of a branched double cover, I*, J. Topol. 7 (2014) 1155–1199 MR

[9] **C Manolescu**, *An unoriented skein exact triangle for knot Floer homology*, Math. Res. Lett. 14 (2007) 839–852 MR

[10] **C Manolescu**, **P Ozsváth**, *On the Khovanov and knot Floer homologies of quasi-alternating links*, from "Proceedings of Gökova Geometry–Topology Conference 2007" (S Akbulut, T Önder, R J Stern, editors), GGT, Gökova (2008) 60–81 MR

[11] **C Manolescu**, **P Ozsváth**, **S Sarkar**, *A combinatorial description of knot Floer homology*, Ann. of Math. 169 (2009) 633–660 MR

[12] **C Manolescu**, **P Ozsváth**, **Z Szabó**, **D Thurston**, *On combinatorial link Floer homology*, Geom. Topol. 11 (2007) 2339–2412 MR

[13] **K Murasugi**, *On a certain numerical invariant of link types*, Trans. Amer. Math. Soc. 117 (1965) 387–422 MR

[14] **K Murasugi**, *On the signature of links*, Topology 9 (1970) 283–298 MR

[15] **P Ozsváth**, **Z Szabó**, *Holomorphic disks and knot invariants*, Adv. Math. 186 (2004) 58–116 MR

[16] **P Ozsváth**, **Z Szabó**, *Holomorphic disks and topological invariants for closed three-manifolds*, Ann. of Math. 159 (2004) 1027–1158 MR

[17] **P Ozsváth**, **Z Szabó**, *On the Heegaard Floer homology of branched double-covers*, Adv. Math. 194 (2005) 1–33 MR

[18] **P Ozsváth**, **Z Szabó**, *Holomorphic disks, link invariants and the multi-variable Alexander polynomial*, Algebr. Geom. Topol. 8 (2008) 615–692 MR

[19] **J Rasmussen**, *Floer homology and knot complements*, PhD thesis, Harvard University (2003) arXiv

[20] **J Rasmussen**, *Knot polynomials and knot homologies*, from "Geometry and topology of manifolds" (H U Boden, I Hambleton, A J Nicas, B D Park, editors), Fields Inst. Commun. 47, Amer. Math. Soc., Providence, RI (2005) 261–280 MR

[21] **S Sarkar**, *A note on sign conventions in link Floer homology*, Quantum Topol. 2 (2011) 217–239 MR

Department of Mathematics, Columbia University
New York, NY 10027, United States
`cmmwong@math.columbia.edu`
`http://www.math.columbia.edu/~cmmwong`